LUND UNIVERSITY

Next generation bioengineering of lung tissue for transplantation

De Santis, Martina M.

2021

Document Version:
Publisher's PDF, also known as Version of record

Link to publication

Citation for published version (APA):
De Santis, M. M. (2021). *Next generation bioengineering of lung tissue for transplantation*. [Doctoral Thesis (compilation), Department of Experimental Medical Science]. Lund University, Faculty of Medicine.

Total number of authors:
1

General rights
Unless other specific re-use rights are stated the following general rights apply:
Copyright and moral rights for the publications made accessible in the public portal are retained by the authors and/or other copyright owners and it is a condition of accessing publications that users recognise and abide by the legal requirements associated with these rights.
• Users may download and print one copy of any publication from the public portal for the purpose of private study or research.
• You may not further distribute the material or use it for any profit-making activity or commercial gain
• You may freely distribute the URL identifying the publication in the public portal

Read more about Creative commons licenses: https://creativecommons.org/licenses/

Take down policy
If you believe that this document breaches copyright please contact us providing details, and we will remove access to the work immediately and investigate your claim.

LUND UNIVERSITY

PO Box 117
221 00 Lund
+46 46-222 00 00

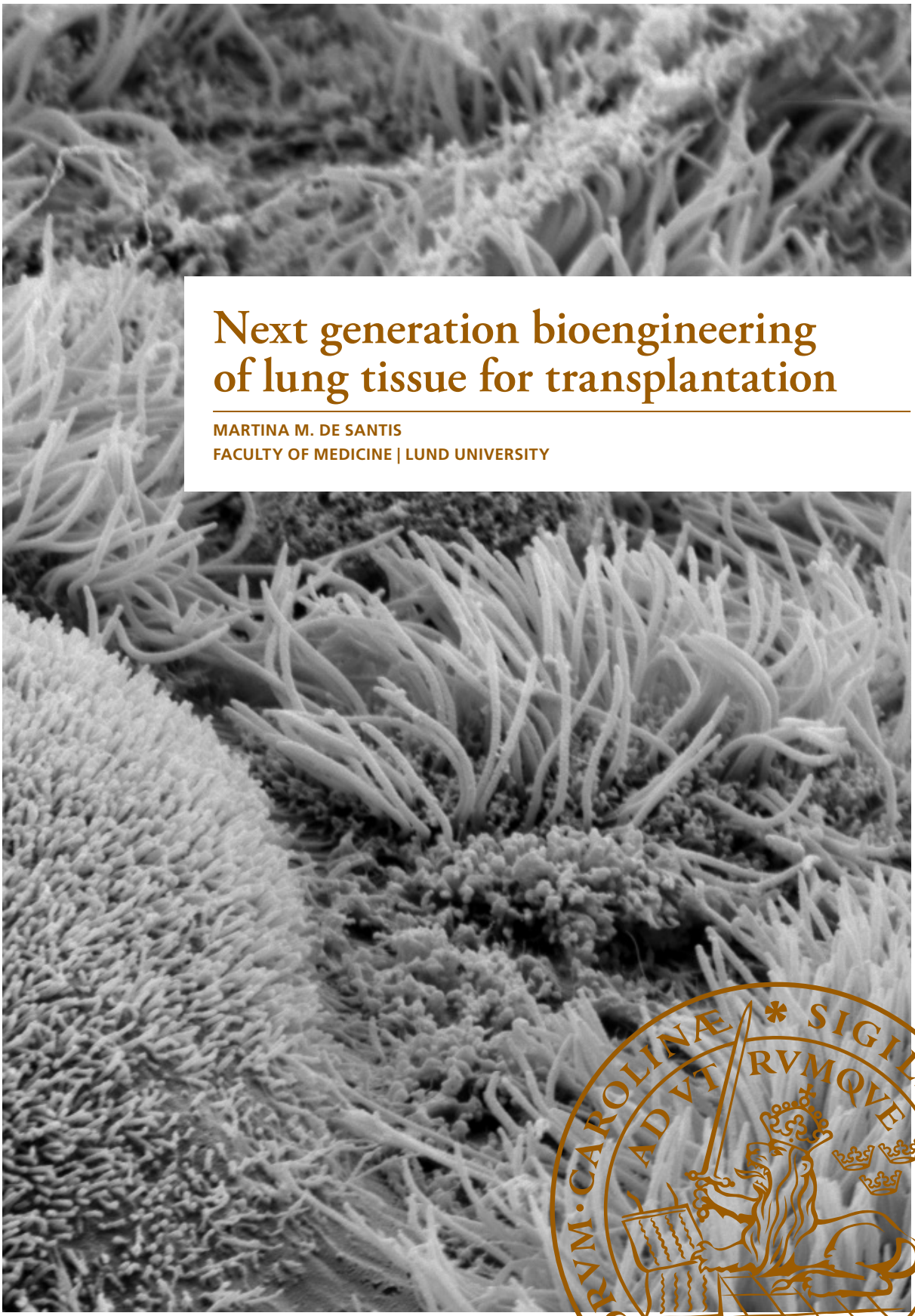

Next generation bioengineering of lung tissue for transplantation

MARTINA M. DE SANTIS
FACULTY OF MEDICINE | LUND UNIVERSITY

Printed by Media-Tryck, Lund 2021 NORDIC SWAN ECOLABEL 3041 0903

About the author

Martina De Santis studied Biochemistry at Imperial College London and then completed her Master's in Biosciences (Stem Cells and Developmental Biology) at University College London. There, she developed her curiosity and passion for bioengineering, bringing her to Lund at the Medical faculty to start a PhD with Darcy Wagner. During her PhD, Martina has been involved in a number of projects that investigate next generation bioengineering solutions for tissue transplantation, gaining experience in *in vivo* and *ex vivo* techniques, *in vitro* 3D cultures, 3D bioprinting skills and imaging techniques. She is looking forward to using her bioengineering expertise to continue solve important biological questions.

LUND UNIVERSITY

FACULTY OF MEDICINE

Department of Experimental Medical Science
Lung Bioengineering and Regeneration

Lund University, Faculty of Medicine
Doctoral Dissertation Series 2021:14
ISBN 978-91-8021-020-1
ISSN 1652-8220

Next generation bioengineering of lung tissue for transplantation

Martina M. De Santis

DOCTORAL DISSERTATION

by due permission of the Faculty of Medicine, Lund University, Sweden.
To be defended at Segerfalksalen A10, BMC, Lund on 19 February 2021 at 14:30.

Faculty opponent
Prof. Sam M. Janes

Organization	Document name
LUND UNIVERSITY	DOCTORAL DISSERTATION
	Date of issue 19 February 2021
Author: Martina De Santis	Sponsoring organization

Title and subtitle: Next generation bioengineering of lung tissue for transplantation

Abstract

Lung transplantation is the only option for end-stage lung diseases, but organ shortage remains problematic. Generating lungs *ex vivo* could overcome shortages with current approaches being explored for lung tissue engineering utilizing a biologically derived, synthetic or hybrid scaffold which is seeded with cells and cultured *ex vivo*. Ideally, cells could be sourced from the transplant recipient and thus are conceptualized to reduce the long-term requirements for immunosuppressive drugs and the risk for rejection. Progenitor cell populations can be controlled more easily than induced pluripotent stem cells (IPSC), with lower risk of tumour formation. However, as presented in this thesis, progenitor cells can be deranged in diseased lungs such as for example idiopathic pulmonary fibrosis (IPF) and are therefore unlikely candidates to generate healthy tissue. In addition to healthy cells, scaffolds with attributes known to be pro-regenerative are required to generate healthy tissues. In the thesis it is shown that both scaffold and cell age plays a role in the regenerative capacity of a tissue. From this it is clear that to generate a healthy tissue or organ, it is critical to find the appropriate scaffold and cell type. Additionally, bioengineering manufacturing methods that generate reproducible, custom-made, high resolution constructs using cytocompatible materials are ideal for tissue engineering approaches. One such method which is compatible with the criteria above and that has emerged in recent years is 3D printing. 3D printing or bioprinting (when cells are printed) can generate custom structures relevant for human lungs. In this thesis, potential bioinks for bioprinting lung tissue are investigated. A tissue-specific hybrid bioink consisting of alginate, reinforced with extracellular matrix from decellularized lung tissue (rECM) was used to 3D bioprint human airways comprised of regionally specified primary cells which remained patent over time. The biocompatibility and vascularisation of rECM hydrogels was investigated in both T-cell immunodeficient mice mimicking the clinical scenario and immunocompetent mice. Bioprinted rECM hydrogels support the formation of an intact vascular network throughout the full thickness of the graft, comprised of both large and small size blood vessels and integrate well in the surrounding tissue.

Key words: bioink; 3D bioprinting; tissue engineering; extracellular matrix; biofabrication; bioengineering

Classification system and/or index terms (if any)

Supplementary bibliographical information		**Language:** English
ISSN and key title: 1652-8220		**ISBN:** 978-91-8021-020-1
Recipient's notes	**Number of pages** 93	Price
	Security classification	

I, the undersigned, being the copyright owner of the abstract of the above-mentioned dissertation, hereby grant to all reference sources permission to publish and disseminate the abstract of the above-mentioned dissertation.

Signature  Date 2021-01-14

Next generation bioengineering of lung tissue for transplantation

Martina M. De Santis

DOCTORAL DISSERTATION

by due permission of the Faculty of Medicine, Lund University, Sweden.
To be defended at Segerfalksalen A10, BMC, Lund on 19 February 2021 at 14:30.

Faculty opponent
Prof. Sam M. Janes

Supervisor: Senior Lecturer and Associate professor Darcy Wagner, PhD

Co-supervisor: Professor Gunilla Westergren-Thorsson, PhD

Co-supervisor: Associate professor Sandra Lindstedt, MD, PhD

Coverphoto by Martina De Santis

Copyright pp 1-93 Martina De Santis

Paper 1 © Advanced Materials

Paper 2 © by the Authors (Manuscript unpublished)

Paper 3 © Nature Cell Biology

Paper 4 © Scientific Reports

Faculty of Medicine
Department of Experimental Medical Science

ISBN 978-91-8021-020-1
ISSN 1652-82-20

Printed in Sweden by Media-Tryck, Lund University
Lund 2021

Media-Tryck is a Nordic Swan Ecolabel certified provider of printed material. Read more about our environmental work at www.mediatryck.lu.se

MADE IN SWEDEN

To my parents

Table of Contents

List of Papers and Manuscripts

Paper I

M. M. De Santis, H. N. Alsafadi, S. Tas, D. Bölükbas, S. Prithiviraj, I. A. N. Da Silva, M. Mittendorfer, C. Ota, J. Stegmayr, F. Daoud, M. Königshoff, K. Swärd, J. A. Wood, M. Tassieri, P. E. Bourgine, S. Lindstedt, S. Mohlin, D. E. Wagner: Extracellular Matrix Reinforced Bioinks for 3D Bioprinting Human Tissue, Advanced Materials, 2005476 (2020)

Paper II

M. M. De Santis, I. A. N. Da Silva, S. Prithiviraj, J. Stegmayr, P. E. Bourgine, D. E. Wagner: Immune response to 3D printed lung derived rECM alginate hydrogels (manuscript)

Paper III

D. Jiang, D. Correa-Gallegos, S. Christ, A. Stefanska, J. Liu, P. Ramesh, V. Rajendran, **M. M. De Santis**, D. E. Wagner, Y. Rinkevich: Two succeeding fibroblastic lineages drive dermal development and the transition from regeneration to scarring, Nature Cell Biology, volume 20, pages 422–431 (2018)

Paper IV

C. Ota, JP. Ng-Blichfeldt, M. Korfei, H. Alsafadi, M. Lehmann, W. Skronska, **M. M. De Santis**, A. Guenther, D. E. Wagner, M. Königshoff: Roles of HOPX in alveolar epithelial cells during the progression of pulmonary fibrosis, Scientific Reports, volume 8, Article number: 12983 (2018)

Abstract

Lung transplantation is the only option for end-stage lung diseases, but organ shortage remains problematic. Generating lungs *ex vivo* could overcome shortages with current approaches being explored for lung tissue engineering utilizing a biologically derived, synthetic or hybrid scaffold which is seeded with cells and cultured *ex vivo*. Ideally, cells could be sourced from the transplant recipient and thus are conceptualized to reduce the long-term requirements for immunosuppressive drugs and the risk for rejection. Progenitor cell populations can be controlled more easily than induced pluripotent stem cells (IPSC), with lower risk of tumour formation. However, as presented in this thesis, progenitor cells can be deranged in diseased lungs such as for example idiopathic pulmonary fibrosis (IPF) and are therefore unlikely candidates to generate healthy tissue. In addition to healthy cells, scaffolds with attributes known to be pro-regenerative are required to generate healthy tissues. In the thesis it is shown that both scaffold and cell age plays a role in the regenerative capacity of a tissue. From this it is clear that to generate a healthy tissue or organ, it is critical to find the appropriate scaffold and cell type. Additionally, bioengineering manufacturing methods that generate reproducible, custom-made, high resolution constructs using cytocompatible materials are ideal for tissue engineering approaches. One such method which is compatible with the criteria above and that has emerged in recent years is 3D printing. 3D printing or bioprinting (when cells are printed) can generate custom structures relevant for human lungs. In this thesis, potential bioinks for bioprinting lung tissue are investigated. A tissue-specific hybrid bioink consisting of alginate, reinforced with extracellular matrix from decellularized lung tissue (rECM) was used to 3D bioprint human airways comprised of regionally specified primary cells which remained patent over time. The biocompatibility and vascularisation of rECM hydrogels was investigated in both T-cell immunodeficient mice mimicking the clinical scenario and immunocompetent mice. Bioprinted rECM hydrogels support the formation of an intact vascular network throughout the full thickness of the graft, comprised of both large and small size blood vessels and integrate well in the surrounding tissue.

Lay Summary

For many patients with end-stage lung diseases, lung transplantation is the only option to save their lives. However, there are not enough lungs to meet the clinical demand. Because of this, many scientists are looking into making new or part of lungs in the lab, also known as lung bioengineering.

In this thesis, key aspects of lung bioengineering and bioengineering as a whole are presented with a focus on 3D bioprinting, that is to print materials together with cells. A material containing cells that can be bioprinted is known as a bioink. Investigating the bioinks, cell types and bioprinting methods that allow for healthy tissue is important. In this thesis, the development of a bioink which can be bioprinted together with lung cells to make small airways is described.

The lung is made out of cells and proteins that support the cells and tells them how to behave (known as ECM). To develop a bioink that is biologically close to lungs, lung ECM is combined with a gel derived from algae that can easily be made into different shapes: alginate. The combination of alginate and ECM results in a bioink which in the thesis is called reinforced extracellular matrix (rECM) bioink. rECM bioinks can be 3D bioprinted together with patient cells into small airways that remain patent over time.

After the bioprinting, the patient cells stay alive and behave consistently to cells in native small airways. When transplanted into mice the structure integrates in the surrounding tissue with blood vessel and capillary formation.

In conclusion, this thesis presents work that is a critical stepping stone for future studies looking into generating tissue via 3D bioprinting and which could result ideally one day into a source of lung tissue for transplantation purposes.

Populärvetenskaplig Sammanfattning

För många patienter med lungsjukdomar i slutstadiet är lungtransplantation det enda livräddande alternativet, men det finns en brist på tillgängliga donatorlungor i förhållande till det kliniska behovet. På grund av detta studerar forskare möjligheten att framställa artificiell lungvävnad i laboratorier, vilket kallas lungbioteknik.

Denna avhandling fokuserat på nyckelaspekter av lungbioteknik och bioteknik, där fokus är på 3D-bioprinting, vilket innebär att man skriva ut 3D strukturer i ett material (så kallat bioink eller biobläck) tillsammans med celler. Det är det viktigt att säkerställa att den 3D-printade vävnaden är livskraftig. I denna avhandling beskrivs utvecklingen av biobläck som kan bioprintas tillsammans med lungceller för att skapa små luftvägar vilka är livskraftiga.

Lungan består av celler och proteiner som stöder cellerna och berättar för dem hur de ska bete sig (vilket kallas som extracellulärt matrix/ECM). För att utveckla ett biobläck som är biologiskt och liknar det naturliga ECM, kombinerades ECM från lunga med ett material som enkelt kan göras till olika former: alginat. Alginat är ett naturligt gelatinliknande matieral som utvinns ur alger. Kombinationen av alginat och ECM resulterar i ett biobläck som i avhandlingen kallas förstärkt extracellulär matrix (rECM). rECM-biobläck kan 3D-bioprintas tillsammans med celler (som isolerats från patienter) till små luftvägar.

Efter bioprintingen förblir patientcellerna levande i den artificiella luftvägen och beter sig som celler i naturliga luftvägar. När de transplanteras in i möss integreras de artificiella luftvägarna med den omgivande vävnaden, och blodkärl växer in i dem.

Sammanfattningsvis presenterar denna avhandling forskning som är av avgörande betydelse för vidare studier av framställning av artificiell vävnad som i framtiden kan utgöra en källa till lungvävnad för transplantation.

Riassunto in Italiano

Per molti pazienti con malattie polmonari allo stadio terminale, il trapianto di polmone è l'unica opzione per salvare le loro vite. Tuttavia, non ci sono abbastanza polmoni per soddisfare la domanda clinica. Per questo motivo, molti scienziati stanno cercando di creare nuovi polmoni usando la bioingegneria polmonare.

In questa tesi, gli aspetti chiave della bioingegneria polmonare e della bioingegneria in generale sono presentati con un focus sulla 3D bioprinting, ovvero la stampa di materiali insieme alle cellule. I materiali che possono essere stampati insieme alle cellule vengono chiamati bioink. È importante studiare i bioink, i tipi di cellule e i metodi di bioprinting che consentono di ottenere tessuti sani. In questa tesi viene descritto lo sviluppo di un bioink che può essere stampato insieme a cellule polmonari per creare piccole vie aeree.

Il polmone è composto da cellule e proteine che supportano le cellule e dirige il loro comportamento (anche conosciuto come matrice extracellulare/ECM). Per sviluppare un bioink che sia biologicamente vicino ai polmoni, l'ECM polmonare viene combinato con un materiale che può essere facilmente trasformato in diverse forme: l'alginato. La combinazione di alginato ed ECM risulta in un bioink che nella tesi è chiamato reinforced extracellular matrix (rECM) bioink. I rECM bioink possono essere stampati in 3D insieme alle cellule del paziente per produrre piccole vie aeree che rimangono stabili nel tempo.

Dopo il bioprinting, le cellule del paziente rimangono in vita e si comportano in modo coerente alle piccole vie aeree native. Quando trapiantato nei topi, il materiale si integra nel tessuto circostante con formazione di vasi sanguigni e capillari.

In conclusione, questa tesi presenta un lavoro critico per studi futuri che esaminano la generazione di tessuto tramite 3D bioprinting e che potrebbe idealmente un giorno essere una fonte di tessuto polmonare a fini di trapianto.

Zusammenfassung in Deutsch

Für viele Patienten mit Lungenerkrankungen im Endstadium ist die Lungentransplantation die einzige Möglichkeit, ihr Leben zu retten. Es gibt jedoch nicht genügend Lungen, um den klinischen Bedarf zu decken. Aus diesem Grund versuchen viele Wissenschaftler, im Labor neue Lungen herzustellen, das auch als Lungen-Bioengineering bezeichnet wird.

In dieser Arbeit warden die wichtigsten Aspekte des Lungen-Bioengineerings und des allgemeinen Bioengineerings vorgestellt, wobei der Schwerpunkt auf dem 3D-Bioprinting liegt, dem Drucken von Materialien zusammen mit Zellen. Materialien die mit Zellen gedruckt werden können, werden auch Bioinks genannt. Die Untersuchung der Bioinke, Zelltypen und Bioprinting-Methoden, die lebensfähiges Organe ermöglichen, ist wichtig. In dieser Arbeit wird die Entwicklung eines Bioink beschrieben, das zusammen mit Lungenzellen 3D gedruckt werden kann, um kleine Atemwege zu bilden.

Die Lunge besteht aus Zellen und Proteinen (bekannt als Extrazellulärer Matrix /ECM), die die Zellen unterstützen und ihnen sagen, wie sie sich verhalten sollen. Um einen lungennahen Bioink zu entwickeln, wird Lungen-ECM mit einem Material kombiniert, das leicht in verschiedene Formen gebracht werden kann: Alginat. Die Kombination von Alginat und ECM führt zu einem Bioink, der in diesem Project als Bioink mit verstärkter Extrazellulärer Matrix (rECM) bezeichnet wird. rECM-Bioinks können zusammen mit Patientenzellen 3D gedruckt werden um kleine Atemwegen zu formen, die im Laufe der Zeit offen bleiben.

Nach dem Bioprinting bleiben die Patientenzellen am Leben und verhalten sich gegenüber gesunde kleinen Atemwegen konsistent. Bei der Transplantation in Mäuse integriert sich das Material mit Blutgefäß- und Kapillarbildung in das umgebende Gewebe.

Zusammenfassend bring uns dieses Projekt dem Bioengineer-Lungengewebe näher, dass idealerweise eines Tages zu einer Quelle für Lungengewebe für Transplantationszwecke führen könnte.

Abbreviations

ALI	Air liquid interface
ATII	Alveolar type II
CAM	Chorioallantoic membrane
COPD	Chronic obstructive pulmonary disease
DCD	Donation after Circulatory Death
dECM	Extracellular matrix hydrogel
DNase	Deoxyribonuclease
ECM	Extracellular Matrix
EdU	5-ethynyl-2′-deoxyuridine
ENFs	Engrailed 1-history-naive fibroblasts
EPFs	Engrailed 1-history-positive fibroblasts
FRESH	Freeform reversible embedding of suspended hydrogels
GAGs	Glycosaminoglycans
H&E	Hematoxylin and eosin
HBECs	Human bronchial epithelial cells
HLSMCs	Human lung smooth muscle cells
IPF	Idiopathic pulmonary fibrosis
IPSC	Induced pluripotent stem cells
M1	Type I macrophages
M2	Type II macrophages
PAH	Pulmonary arterial hypertension
PERV	Porcine endogenous retrovirus
rECM	Reinforced extracellular matrix hydrogel
SEM	Scanning electron microscopy
TBM	Tracheobronchomalacia

Introduction

Lung diseases and transplantation

Chronic respiratory diseases such as idiopathic pulmonary fibrosis (IPF), chronic obstructive pulmonary disease (COPD), cystic fibrosis, pulmonary hypertension, lung cancer and asthma are the third leading cause of death worldwide with an overall EU cost of more than €380 billion annually.[1] Overall, 4 million people die prematurely of chronic lung diseases per year.[2] Lung cancer, one of the most common neoplasms, may be cured if identified in the early stages, but has generally low survival rates with 1.6 million people dying each year.[3] Mild to moderate asthma affects 334 million and is prevalent in 14% of all children globally and can be controlled with steroids or bronchodilators.[4] However other respiratory diseases do not have curative options. An estimated 65 million people suffer from COPD worldwide, and 3 million patients die per year.[5] The only option for end stage respiratory diseases is lung transplantation with about 2000 lung transplants occurring in Europe per year.[6] A large discrepancy exists between the number of organs needed and the number available, thus strict regulations are used to prioritize who will obtain a transplant. Moreover, the efficacy of the transplant remains a significant clinical issue as transplant rejection rates are high and complications can arise due to the required immunosuppressive drugs resulting in only half of the transplanted people surviving 5 years. This is the lowest survival rate for any solid organ.[7]

It is clear that alternative options are needed to increase available lung tissue for transplantation to address the shortage of donor organs. An exciting new area of research has emerged in recent years that focuses on generating lung tissue *ex vivo* also known as lung bioengineering.[8]

Architecture of the lung

The lung is the major organ of the respiratory system, and in humans is composed of 5 lobes. The right lung is composed of three lobes and is slightly larger than the left lung, which instead has two lobes. With each inhalation, air is pulled first through the trachea, passing through the bronchi, into the alveoli. Tiny capillaries are present in the walls of the alveoli, allowing for the transfer of oxygen from the

air inside the alveoli to the red blood cells (erythrocytes) of the blood and further onto the rest of the body. Erythrocytes release the oxygen and pick up carbon dioxide which is carried back through circulation to the alveoli. By exhaling, carbon dioxide is expelled from the bronchi out of the body through the trachea. For optimal function of the lungs at least 40 different resident cell types are required.[9-12]

Lung epithelial cells

Lung epithelial cells are known to play a fundamental role as a central regulator for lung diseases and have been shown to be altered by cigarette smoke[13,14] and deranged in major lung disorders such as COPD[15-17], asthma[18], cystic fibrosis[17,19] and IPF[20,21]. Epithelial cells cover the airways which in the adult human bronchial tree is the major line of defence against inhaled particles and microbes[22-24]. The airway epithelium is pseudostratified in the large airways and columnar and cuboidal in the small airways and is comprised of multiple epithelial cell types which include ciliated cells, goblet cells, intermediate cells, neuroendocrine and basal cells. In healthy adult human lungs the presence of certain epithelial cells differ depending on the location in the airways, with a higher incidence of club cells in the small airways and cartilage cells and submucosal glands in the large airways (Figure 1)[25].

Basal cells, positioned directly on top of the basement membrane, are cuboidal progenitor cells which may differentiate into ciliated or goblet cells in case of injury. The airways are lined with a layer of mucus, produced by goblet cells and submucosal glands, which is transported upwards to the pharynx by coordinated ciliary beating of ciliated cells[26]. This mechanism, also known as the mucociliary clearance, is critical for eliminating pathogens and foreign particles from the airways and if deranged can contribute to the pathogenesis of serious diseases such as pulmonary fibrosis[27]. In addition to mucociliary clearance, the lungs have an additional barrier in the tight and adherens junctions formed between neighbouring cells in the airway epithelium.

Other cells present in the large and small airways are intermediate cells which are believed to be in a transition between basal cells and the terminally differentiated cell types, and the recently discovered pulmonary ionocyte which is hypothesized to play an important role in the pathology of cystic fibrosis[28].

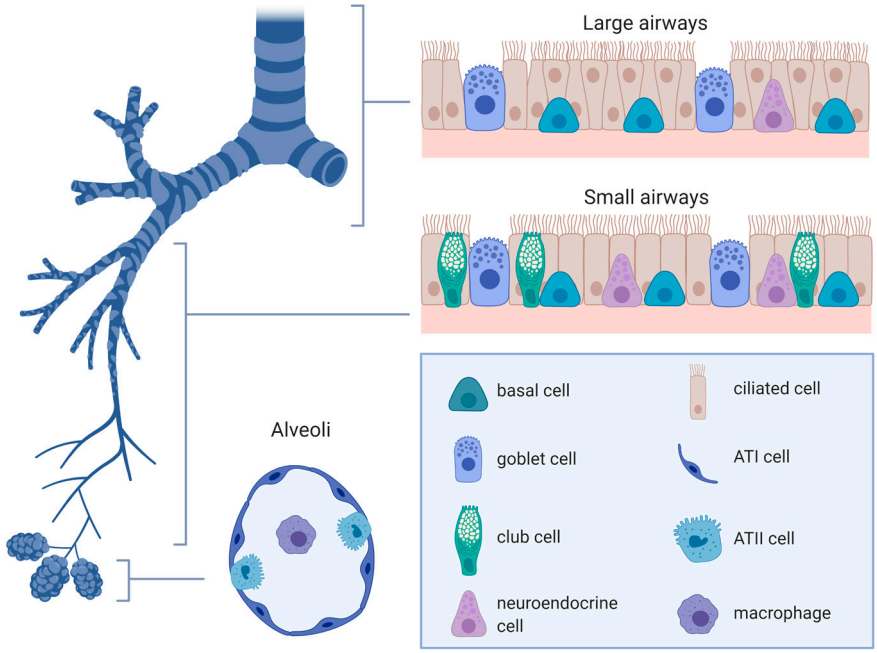

Figure 1 Major cell types of the lung epithelium

The presence of certain epithelial cells differs depending on the location in the lung. Ciliated, intermediate, goblet and basal cells are present in the large airways (20 to 25 branches) with a higher number of ciliated cells and club cells present in the small airways (26 to 223 branches), After 223 branches, the airway epithelium merges with the alveolar epithelium comprised of alveolar type I (ATI) and type II (ATII) cells and alveolar macrophages. The most recent concept of human alveoli postulates only one ATI cell covering the surface area with one or two ATII cells and one alveolar macrophage present. The figure does not show ionocytes, intermediate and cartilage cells and mucus glands present in the large airways. Created with BioRender.com

Various cell markers which can be used to identify and differentiate between the airway epithelial cells, have been confirmed by recent single cell RNA sequencing studies (Table 1). Transcription factor forkhead box J1, also known as FOXJ1, is a transcription factor involved in controlling the differentiation towards the ciliated cell lineage and is used together with acetyl alpha tubulin as a ciliated cell marker[29-32]. Mucin5ac (MUC5AC) and to some extent Mucin5b (MUC5B) (also secreted by submucosal glands) are instead expressed in goblet cells[33]; keratin 5 (KRT5), keratin 14 (KRT14) and p63 are used as basal cell markers[34] and CC10 as a club cell marker[35,36].

The airway epithelium transitions to the alveolar epithelium which consists of alveolar type I cells which cover ~ 95% of the alveolar surface and alveolar type II cells, progenitor cells of the alveolus and important for pulmonary surfactant production[25]. ATI cells are vital for gas exchange and alveolar-capillary barrier function[37]. In addition, alveolar macrophages are also present which help clear noxious particles which have escaped the defences from the respiratory tract and

help to resolve inflammation in the air spaces[38]. Markers for alveolar epithelial cells include HOPX and aquaporin 5 (AQP5) for ATI cells[39] and surfactant protein C (SP-C) for ATII cells[40].

Table 1 Major cell markers of the lung epithelium

Markers	Cells
KRT5, KRT14, p63	Basal cells
FOXJ1, Acetyl α-tubulin	Ciliated cells
MUC5AC, MUC5B	Goblet cells
CC10	Club cells
HOPX, AQP5	ATI cells
SP-C	ATII cells

Airway smooth muscle cells

Airway smooth muscle cells are present in the respiratory tract and control the airflow resistance in the airway.[41-43] They are found on top of the cartilage and form dense bundles in airway walls between the mucosa and submucosa. As the airway diameter decreases going from large to small airways, the airway smooth muscle cells cover a larger portion of the cross section of the airways and change their orientation from transverse to helical-antihelical[44]. Airway smooth muscle cells are surrounded by complex protein networks including reticular fibers and collagens which allows them to reduce the airway luminal diameter when contracting after exposure to allergens or toxins. This can then result in airway hyper responsiveness and acute airflow obstruction and other symptoms characteristic of asthma.[45]

Tissue Engineering

Tissue engineering is an interdisciplinary field that was first described by Langer and Vacanti as a field that "applies the principles of engineering and life sciences toward the development of biological substitutes that restore, maintain, or improve tissue function or a whole organ"[46]. In the postulated "triad of tissue engineering" starting points for creation of new tissue are described as combining cells with a scaffold matrix and with the assistance of tissue inducing substances[46]. However, the field now also encompasses acellular scaffolds or biomaterials which aim to recruit cells upon implantation and are designed to direct *in vivo* remodelling of the implanted biomaterial which ultimately leads to regeneration. To date, there have

been several studies and clinical trials which have shown the feasibility of using tissue engineering products and approaches in the clinic.[47,48] Approaches for skin tissue engineering, utilising acellular skin grafts, are now used clinically, whereas other tissues, including lung, are still in earlier research stages. Lung tissue engineering approaches have adopted similar paradigms to other tissue engineering approaches in which cells are combined with natural, synthetic or hybrid matrices, and grown *ex vivo* before hypothetical transplantation (Figure 2).

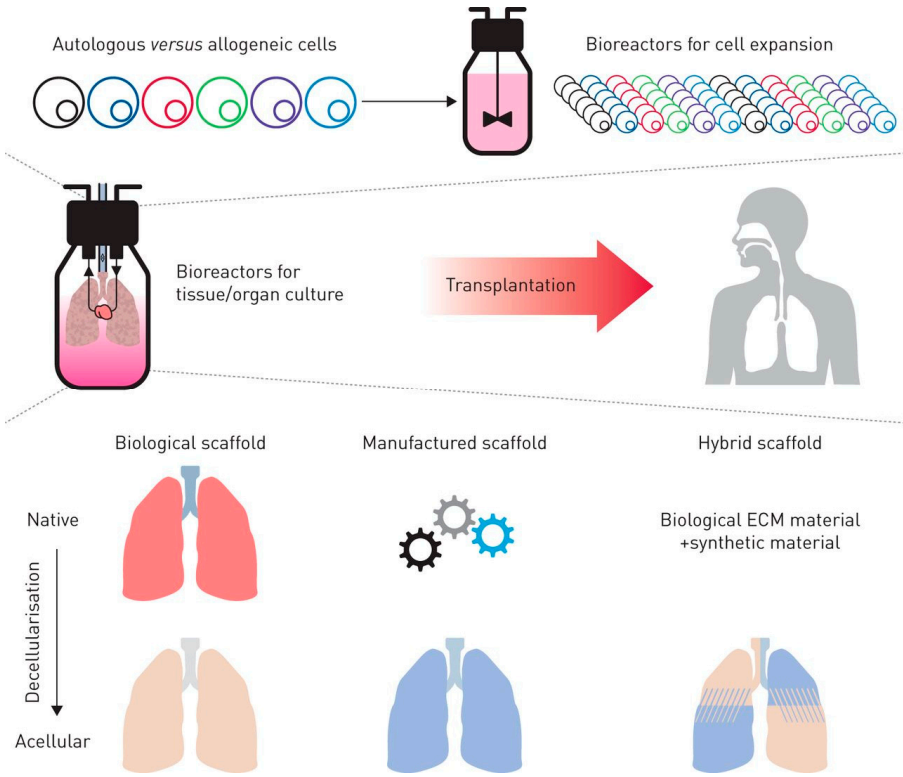

Figure 2 Lung Bioengineering approaches

Lung scaffolds can be seeded with fully differentiated or progenitor autologous or allogeneic cells, which can be expanded to appropriate cell numbers in bioreactors for cell expansion. Lung scaffolds used for lung bioengineering approaches include acellular (decellularized) scaffolds, synthetic scaffolds and more recently hybrid scaffolds made out of a combination of biological materials and synthetic materials. Recellularized lung scaffolds can then be matured in bioreactors for organ culture before lung transplantation. Figure reproduced from De Santis et al, 2018 with permission.[8]

Autologous cells, derived from the eventual transplant recipient, may be regarded as an ideal cell source for recellularising lung scaffolds. These cells could be either fully differentiated adult cells or progenitor cells which could be directed to differentiate into the different cell types found in healthy lungs. Using autologous cells or immunologically matching cell types (i.e. by HLA-compatible) is ideal as this would minimise post-transplantation immune complications and the long term need for immunosuppressive drugs. In addition to immunological matching, the disease status of the autologous cells is also of importance as we and others have

found that progenitor cells can be deranged in diseased lungs such as for example idiopathic pulmonary fibrosis (IPF)[20] (paper IV) and therefore the likelihood is low that these could be used to generate healthy tissue. Another option would be to use induced pluripotent stem cells (IPSC) from the eventual transplant recipient. To date, there are several established protocols for deriving different lung epithelium cell types from both the large airways as well as distal gas exchange regions.[49-56] However, as is the case with embryonic stem cells (ESCs) concerns with tumour formation remain.[57,58] In addition to sourcing healthy cells, scaffolds with attributes known to be pro-regenerative are required to generate healthy tissues. Interestingly, we found that the age of the scaffold and the age of cells can play a role in the regenerative capacity of a tissue (paper III).[59] From this it is clear that to generate a healthy tissue or organ, it is critical to find the appropriate scaffold and cell type.

Extracellular Matrix

In native tissue, cells reside on and within what is called the extracellular matrix (ECM). The ECM is comprised of different secreted products which are maintained during homeostasis by resident cells. These secreted products represent a diverse mix of structural and functional proteins, glycoproteins and glycosaminoglycans (GAGs) whose combination is unique to each anatomic location. The ECM acts together as a scaffold to provide structure and to direct repair and regeneration after injury[60,61] by controlling cell behaviour such as migration, proliferation and differentiation[6,62,63]. For this to happen, the ECM must exist in a state of dynamic reciprocity with the resident cells.[61] Meaning, the composition and organization of the ECM changes depending on the metabolic adaptations of the cells which in their turn change depending on the mechanical properties, pH, oxygen concentration, and other variables in the microenvironment.[61] Therefore, the ECM with its dynamic interactions with the cells has evolved to be the ideal scaffold for resident cell populations including those in the lung.

The organization of the lung ECM is similar to other organ systems, with an organization into two main structural types.[60] The first being the basement membranes, composed of thin glycoprotein sheets which cover the basal side of the epithelia and endothelia, and surround muscle, fat and peripheral nerve cells.[60] The second being interstitial matrices which is maintained by the activity of resident fibroblasts, forming a loose and fibril-like meshwork interconnecting the different structural cell types.[64] Collagens are the major ECM protein component of the lung[65], and are severely altered in many lung diseases (Figure 3).[66] Fibrillar collagens (types I, II, III, V and XI), contribute to the structure of the lung by having great tensile strength but low elasticity.[67,68] Elastins forming elastic fibers have low tensile strength but high elasticity, and thus provide the lung with the necessary compliance and elastic recoil required for breathing.[69]

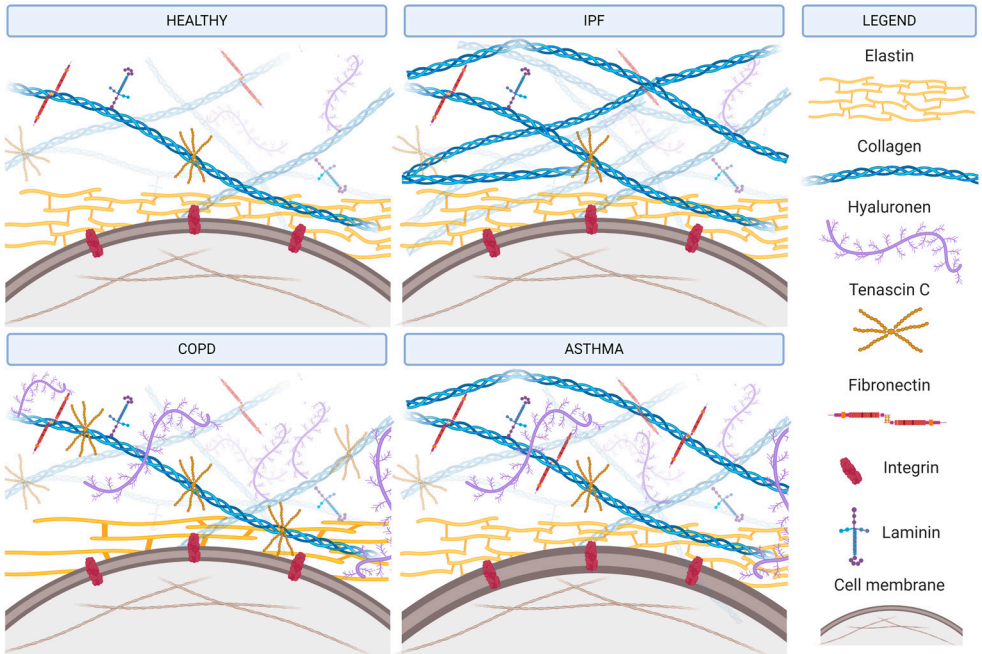

Figure 3 The ECM in healthy and diseased lungs

Pathological changes within the interstitial extracellular matrix (ECM) in healthy and diseased lung. Created with BioRender.com

In lung diseases, the ECM is increasingly recognized as aberrant. Fibroblasts can transdifferentiate into highly contractile myofibroblasts in lung diseases such as IPF, and deposit high levels of collagens and other matrix proteins into the interstitium, resulting in pulmonary fibrosis. The rigidity of the matrix due to the covalent crosslinking collagens and elastins is also dramatically increased and also leads to a decrease in gas exchange capability due to thickening between the airspaces and capillaries as well as a general loss of surface area.[60] In COPD, instead, elastic fibers and subsequently the alveolar septae are degraded by enzymes released by inflammatory cells. Higher levels of hyaluronan and tenascin C are also released by inflammatory cells and decorin is deposited less.[70] The resulting air space enlargement seen in COPD, also known as emphysema, occurs due to the destruction of the elastin and collagen which form the alveolar septae.[68] The vascular ECM is remodelled in pulmonary arterial hypertension (PAH), with an increase in elastin and collagen fibres, fibronectin, and tenascin C in the arterial wall.[60] On other hand, in asthma, ECM changes occurs beneath the bronchial epithelium and thickened basal membrane; with hyperplasia of smooth muscles and increased deposition of ECM such as collagens, fibronectin, hyaluronan and decorin.[71,72] In cancer, tumours are surrounded by highly crosslinked collagens, high levels of fibronectin, tenascin C and hyaluronan resulting in a stiff stroma. From the

above it is clear, that the composition and organization of the ECM will be critical when finding an appropriate lung scaffold.

Decellularization

One method to access the ECM is through decellularization to generate acellular tissue specific scaffolds. Decellularization is defined as the "removal of cells from a tissue or an organ leaving the complex mixture of structural and functional proteins that constitute the ECM".[73] Protocols to generate decellularized lungs and airways have been described by several groups and rely on similar principles of decellularising other organs by using different combinations of physical, ionic, chemical and enzymatic solutions.[74] Detergent-based solutions are the most prevalently utilised for decellularising lungs. Commonly used detergents include Triton X-100, sodium deoxycholate (SDC) and sodium dodecyl sulfate (SDS). These detergents are used either with or without hypertonic sodium chloride and DNase and/or RNase solutions and at different concentrations and volumes depending on the protocol and the species.[6,8,75-84] Perfusion of the solutions occurs either only through the vasculature or both through the airways and vasculature. Variations between different protocols for decellularising lungs has resulted in differences in histology and retention of ECM.[82,85,86] Nevertheless, most laboratories, including ours, utilise the criteria set forth by Crapo et al. to determine effective decellularization of acellular lung scaffolds. The criteria includes (1) absence of visible cellular or nuclear material on histological examination, (2) less than 50 ng dsDNA per 1 mg of dry weight of the ECM scaffold, and (3) remnant DNA shorter than 200 bp.[62] Whilst, the criteria is a good starting point for acellular lungs it does not take into account cytocompatibility (*e.g.* whether residual decellularising agents or unremoved cellular components affect the viability of cells), composition (e.g. ECM retention), and mechanical properties of the acellular scaffold, all important aspects to consider for recellularization.[8,87,88]

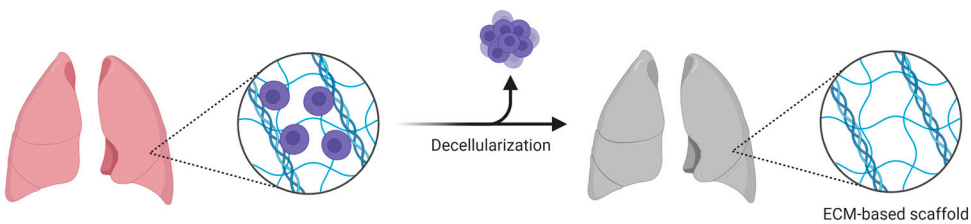

Figure 4 Lung decellularization

Harvested murine and human lungs are decellularized using a combination of detergents and enzymes (described above) which remove the native cells and DNA but retain the extracellular matrix. Created with BioRender.com

Acellular scaffolds

Acellular lung scaffolds retain, to a large extent, the complex structure and the macro- and micro-architecture of native lung tissue. This is of great advantage, as to date, no manufacturing techniques are capable of generating the complex native ECM structure to the same degree observed in acellular lungs. Even though most ECM components are retained in acellular scaffolds[62,89,90], their quantity and the retention of their native orientation is not fully known.[8] This is of importance as the retention and organisation of ECM components, will likely influence the functionality of the bioengineered tissue.

Another source for clinical acellular lungs, could be lungs from anatomically similar species, such as porcine or non-human primates. Using scaffolds from these alternative donors could lead to a more uniform scaffold, with less limitations than scaffolds derived from human sources.[78,79,89,91-93] However, there are ethical concerns with using non-human primate lungs as a source of acellular scaffolds[8] and pleural blebs have been shown to arise in porcine lung scaffolds during decellularization. Pleural blebs could affect the ventilation mechanics of the lung, and ultimately if ruptured would lead to a pneumothorax (e.g. a collapsed lung).[78,81] Moreover, porcine lungs have less collateral ventilation compared to humans which could compromise the function of the lung if transplanted.[8] In addition to this, residual, cell-associated xenogeneic proteins are present in porcine acellular lung scaffolds which may cause negative immunogenic responses in humans.[62,93]

Furthermore, potential retention of zoonotic viruses remain a major concern for the clinical use of xenogeneic tissues.[94] Currently, it is not known whether it is possible to remove zoonoses, such as porcine endogenous retroviruses (PERVs), in xenogeneic acellular scaffolds and thus the danger of cross species transmission of PERVs is not known.[84] From the above it is likely that, adult human lungs which narrowly miss the criteria for transplantation will likely be the best candidates as a scaffold source for clinical grade lung tissue bioengineering.

3D Bioprinting

The lung architecture depends on the location within the lung: moving from proximal (trachea) to distal (bronchi and alveoli), the resolution required to mimic the native structures increases (centimetres (cm)→micrometres (μm)→nanometres (nm)) (Figure 4).[8] As a simplistic notion, the lung parenchyma is formed by interconnected porous structures surrounded by capillaries required for gas exchange.[23] To engineer such porous structures, different manufacturing methods have been used such as freeze drying, solvent-casting, foaming, and particulate-leaching techniques.[8,95] In addition to this, perfusable vascular channels have been fabricated using such methods in tissue engineered constructs.[96]

Manufacturing methods which allow for custom-made, reproducible, 3D designs using cytocompatible materials are ideal for tissue engineering. One such approach, is 3D printing (bioprinting when cells are printed), and has emerged as a source for bioengineering tissues or supporting structures.[97-103] 3D printing was first developed in the 1980's with the concept of stereolithography, where 3D computer-aided designs could be converted into physical constructs by projecting light patterns into a bath of photopolymers.[104] Other 3D fabrication strategies emerged quickly after, including fused deposition modelling (FDM) in the late 1980's, which fabricated 3D constructs by precisely depositing layers of molten thermoplastic in a successive fashion using a mobile heated nozzle.[105,106] To date, FDM is the most popular 3D printing technique. Due to its low cost and accessibility (and its patent expiration), FDM has become very popular.[106] Open source designs like RepRap printers ("Replicating Rapid-Prototyper"), have dramatically decreased printer costs from the tens of thousands of euros to fewer than 200 euros, bringing 3D printing into the hands of millions of hobbyists and academics.[106]

The accessibility of 3D printing has brought the technology to new fields, including regenerative medicine. 3D printing has been applied to replicate patient anatomy for simulation procedures, custom prosthetics and in the case of the lung for treating tracheobronchomalacia (TBM)[107] and tracheal collapse by 3D printing patient-specific tracheal splints[108]. Most recently, 3D printing has been adopted not only for supporting structures but also for bioengineering with the goal of developing cell-laden scaffolds to enable patent human tissue to be regrown from a patient's own stem cells. This 3D printing method using cells is called "3D bioprinting" and the cell-laden material a "bioink".[109,110] Examples of 3D printed tissue engineered organs and tissues include rat tracheas[111], cartilage[112], skin[113], aortic valve conduits[114], and vascular tissue[115]. 3D bioprinting distal lung tissue will be challenging, due to the gas exchange barrier being around the order of nanometres and the nozzles utilised for bioprinting being in the micrometre range to allow for cell passage. It is clear, that new 3D printing or manufacturing approaches need to be developed to overcome this limitation.[8] Nevertheless, current 3D printing technologies can print structures at the resolution of trachea and bronchus, and our lab has described materials and manufacturing methods compatible with cells for bioprinting sizes down to small airways (paper I).

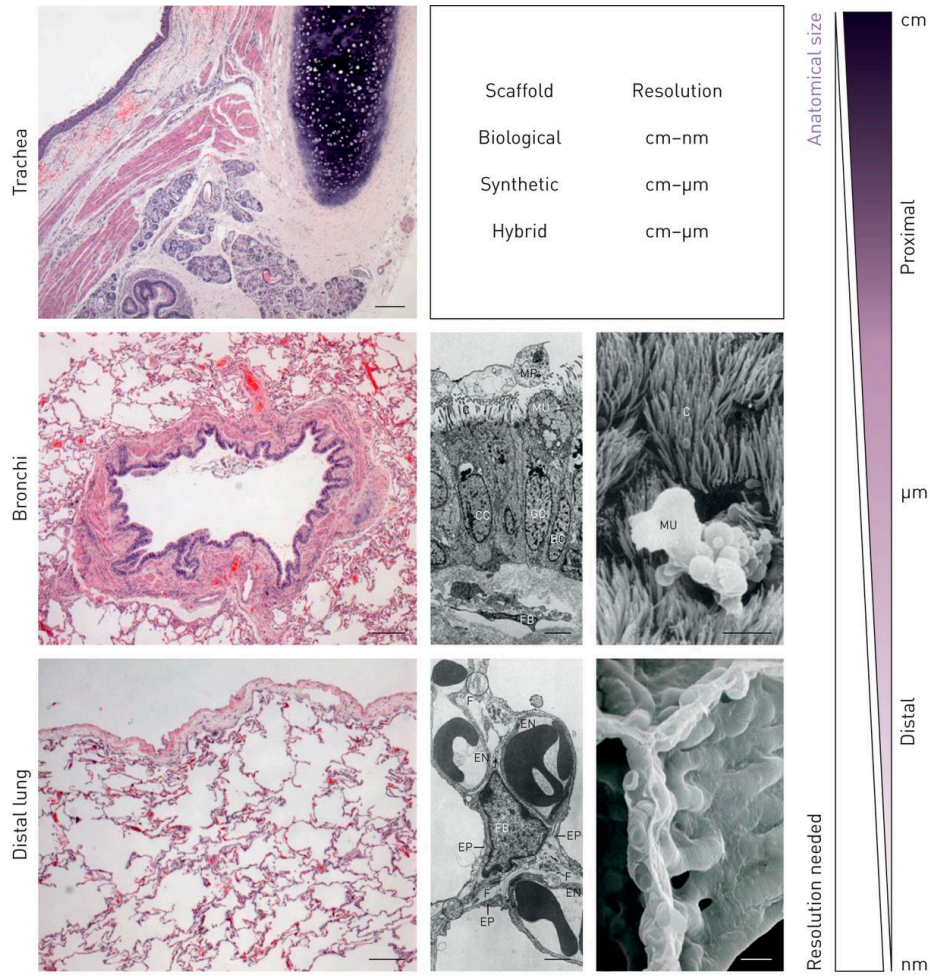

Figure 5 Recapitulating the complexity of the lung architecture from proximal (trachea) to distal (bronchi and alveoli)

Haematoxylin/eosin (H&E; left column) staining histology, transmission electron microscopy (TEM; centre column) and scanning electron microscopy (SEM; right column) images from proximal and distal native lung tissue. The bronchi TEM micrograph of a thin section of the mucous membrane of a small human bronchus shows a ciliated cell (CC) with cilia (C) and microvilli, a goblet cell (GC) with an apical mucous plug (MU), basal cell (BC), fibers and fibroblasts (FB) in connective tissue and macrophages (MP). The bronchi SEM micrograph of the epithelial surface shows ciliary tufts (C) and a mucous plug (MU) of a goblet cell in the process of extrusion. The distal lung TEM and SEM micrographs of the structure of the alveolar septum in human lungs show a septal fibroblast (FB), capillary endothelium (EN), alveolar epithelium (EP) and fiber strands (F). HE histology scale bars: 100 µm; bronchi TEM scale bar: 5 µm; bronchi SEM scale bar: 10 µm; distal lung TEM scale bar: 2 µm; distal lung SEM scale bar: 10 µm. Electron microscopy images reproduced and modified from [116,117] with permission. Figure and text reproduced from De Santis et al, 2018 with permission.[8]

Support baths

Traditional 3D printing utilises solvents or heating to allow for the polymer solutions to flow as liquids through the 3D printing nozzles. This is a major challenge for 3D bioprinting biological tissue as the high temperatures used (in excess of 60°C depending on the polymer) are incompatible with the cells and most biological materials. Thus, it is not advisable to use high temperatures to melt and cure bioinks. Light-induced curing, commonly used in tissue engineering approaches, could be used instead for curing bioinks as it is rapidly improving in print resolution, and is cytocompatible.[118] Yet, with light-induced curing during bioprinting, cells are exposed longer to photo-initiators, which can be cytotoxic.[98] Additionally, light-based curing is mostly performed in air for high print fidelity and for high transmission of light, which can lead to dehydration and cell death.[118] Due to the limitations described above, different bioinks with alternative curing processes have been investigated.[97,98,119,120]

Many of these alternative curing processes involve the printing of the bioink in a support bath which provides a semisolid medium to print into, circumventing many of the issues of printing onto a flat surface in air. Support baths have been reported to be made out of low concentration microgels[120], gelatin slurries[98], modified hyaluronic acid supramolecular hydrogels[119], granular gels[97] and nanoclay hydrogels[121]. These support baths exhibit solid-like characteristics in the absence of an applied stress or at very low stresses.[97,119,122,123] Once a stress is applied that overcomes the yield stress, the support bath will exhibit liquid-like properties.[123] This behaviour is characteristic of Bingham plastics.

Additionally, many support baths are self-healing, meaning they are displaced by the nozzle during printing, but soon after their microstructure spontaneously recovers.[123] Therefore, self-healing allows the transition from a liquid-like state back to a solid-like state, encapsulating the deposited ink.[124] To increase resolution, fluidization of the support bath should be rapid so that crevasses or air pockets are avoided.[125] As a result, support baths permit printing soft materials or low-viscosity fluids, thus, noticeably increasing printable materials with extrusion-based printing techniques, such as for example hydrogels.

FRESH printing

One bioprinting technology that uses support baths is the freeform reversible embedding of suspended hydrogels (FRESH) technique, which involves printing the bioinks into a gelatin slurry. The gelatin slurry can be modified to contain divalent cations such as Ca^{2+} ions to ionically crosslink bioinks. The FRESH printing method allows for the ionic crosslinking to occur gradually whilst the gelatin slurry holds the construct in place. This permits for more complicated shapes with higher resolution compared to other 3D bioprinting methods.[98]

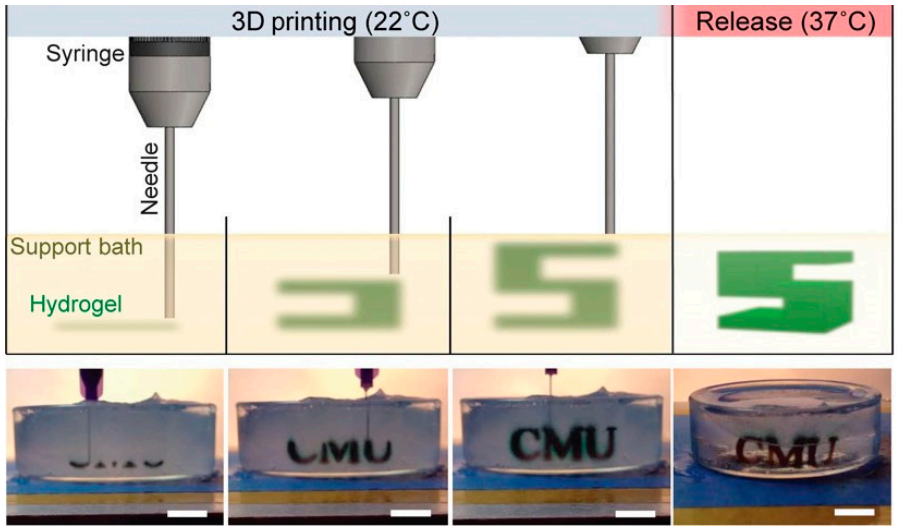

Figure 6 FRESH printing process

Hydrogel based bioinks are typically in a liquid-like state, making it impossible to support subsequent layers. Yet, when combined with support baths, complex structures can be printed. The hydrogel bioink is extruded and cross-linked in the gelatin slurry support bath. The support bath allows for the 3D construct to be built layer by layer. Gelation occurs in the gelatin slurry through one of multiple cross-linking mechanisms. When completed the construct is released by heating to 37°C and melting the gelatin. Figure reproduced from Hinton et al, 2015 with permission.[98]

Bioinks

Due to the cell-friendly nature of hydrogels, they have become the basis of almost all bioink formulations.[106] Hydrogels are highly hydrophilic polymers which are loosely crosslinked. Moreover, hydrogels are mostly constituted by water with water content ranging from 70% to over 99%, making them highly porous and permeable, thus permitting rapid diffusion of oxygen and nutrients throughout the scaffold.[106,126,127] Additionally, many hydrogels are porous and thus allow cell migration, important for initial cell remodeling and regeneration but also for longer term tissue or organ function. Most hydrogels currently used in biomedical research are randomly crosslinked hydrogels, with no internal mechanism for mechanical energy dissipation. These “conventional” hydrogels are cytocompatible but lack mechanical properties required for optimal 3D printing. Research focused on adapting “conventional hydrogels” for 3D bioprinting is therefore emerging. Proteins and extracellular matrix components, including collagen and hyaluronic acid (HA) can also be used as building blocks for hydrogels, providing an environment which contains biological cues that can help direct cell growth, differentiation and migration. Important for cell viability, many hydrogels can be crosslinked into solid viscoelastic structures using methods such as ionic crosslinking or temperature based self-assembly which do not damage and minimize

the physiological stress on bioprinted cells. All the characteristics above allow hydrogels to closely mimic the native ECM of cells, and thus they have been widely used for 3D bioprinting.[127-129]

Alginate

One potential hydrogel based bioink which has been extensively explored in previous 3D bioprinting studies is sodium alginate.[130] Alginate is a cytocompatible polysaccharide extracted from brown seaweed and is already used in clinics for dermal wound healing purposes.[131] Sodium-alginate solutions are known to be shear thinning and can be fast and easily crosslinked with the addition of divalent cations to form hydrogels.[132,133] Even though, alginate has already been used for bioprinting approaches, it is generally regarded as biologically inert to mammalian cells[132,134] and does not mimic the native environment of the lung. ECM components have been previously added to alginate solutions[135] and have been shown to confer enhanced biological properties to seeded cells. Recent work has also indicated that despite its 'inert' biological properties, alginate can facilitate the growth of intestinal organoids derived from pluripotent stem cells, which contain both epithelial and mesenchymal cells.[136] However, epithelial only organoids failed to expand in alginate (even when formed first in Matrigel) and this was attributed to altered polarization of epithelial cells as compared to those grown in Matrigel. This demonstrates that while alginate can support organoid formation, including in three dimensions, that it lacks specific cues needed for inducing other biological cues such as polarization.

dECM solutions

ECM components can be extracted from various decellularized organs using either acidic or enzymatic conditions (e.g. pepsin). When extracted properly to retain collagen peptides of proper size and under appropriate temperature, pH and salt conditions, these solutions can self-assemble to make tissue derived ECM hydrogels. These solutions are termed decellularized ECM solutions (dECM). So far, tissue derived ECM hydrogels have been generated from various tissues, including the intestine[137], lung[138], dermal tissue[139], brain[140] and urinary bladder matrix[90] but reproducibility remains an issue.[141] Furthermore, manufacturing of complex shapes with high resolution is very difficult with ECM hydrogels as the gelation time takes around 10-30 minutes and they remain too weak for structures taller than a few millimeters.[138] ECM hydrogels can be strengthened by increasing their polymer content but it is important to note that the permeability and porosity that the cells need decrease with higher polymer content. dECM solutions have also been chemically modified through the addition of methacryl groups to facilitate covalent crosslinking, but this can bring additional cytotoxic effects if used as a bioink and these materials require further optimization.[142]

Hybrids

In many manufacturing fields, optimal materials are derived through the use of hybrid or composite materials whereby the positive attributes of two or more materials can be combined to generate a final material with optimal overall properties which overcome the limitations of the individual components it is comprised of. Using hybrid or composite materials to manufacture scaffolds or bioinks might therefore be an ideal solution as the biologically conducive nature of the ECM-derived scaffold material, such as sites for cell adhesion and organisational and differentiation cues, could be combined with synthetic materials and advanced manufacturing approaches to produce more reproducible products with tunable or controllable mechanical properties.

Bioprinting has made substantial advances in the past two decades, yet bioinks which mimic the physiological microenvironment of the lung have not been fully explored. A current limitation to most commercial bioinks is that they are lacking in true ECM-like components.[143] This can prevent cells from recognizing and interacting with their microenvironment as well as restrict the development of *in vivo*-like tissues and morphologies. Bioinks can be optimized by combining previously characterized biomaterials with physiologically relevant materials that cells will recognize as actual ECM rather than inert or synthetic alternatives[143-149]. In this thesis, I describe the development of a new bioink for pulmonary tissue engineering which combines the reproducibility of engineered materials with the biologically inductive properties of the native lung extracellular matrix (ECM) and its associated proteins.

Validation methods

Some hydrogels are degradable, which can be an advantage as they can support cells initially and then once the cell populations grow and remodel their surroundings, they degrade, leaving behind a more natural environment.[106] It is important that the printed material does not degrade before new ECM is synthesized, deposited and organized by the seeded cells, as the structure of the tissue needs to be supported and any mechanical loading handled (e.g. further cell seeding, bioreactor parameter, surgical handling and tissue function).[150] Thus, the degradation kinetics and the impact of the degradation products are important parameters to consider when selecting, designing and validating potential new bioinks. Confocal microscopy is a good validation method to investigate material degradation over time and to assure print fidelity.

Additionally, commonly used bioinks do not contain tissue specific cues. Each tissue requires distinct biological, mechanical and architectural properties for proper function, therefore, development of functional tissue using 3D bioprinting will require the development of tissue specific bioinks. Other validation methods used in the thesis can be found below.

Cell sedimentation

As we move closer to printing clinically relevant full-scale tissues and organs, the times required for bioprinting will be very long. Thus, cells may need to remain suspended in bioinks for very long time periods, with a risk of cell sedimentation to the bottom of the cartridge.[118] Utilising a bioink that is viscous enough to maintain a homogeneous distribution of encapsulated cells with little to no cell sedimentation is desirable. Additionally, cell sedimentation can also reduce the resolution and overall quality of the print due to printhead clogging. In this thesis we have used a protocol previously developed[118] to quantify cell sedimentation.

Shear thinning

In addition to cell sedimentation, another key parameter affecting the overall bioprinting is the flow profile of bioinks. When cells travel through an extrusion needle, different types of flow profiles can be experienced depending on the bioinks. Some flow profiles are more "cell friendly" whilst other are less cytocompatible and ultimately lead to cell membrane damage and death. An advantageous flow profile is achieved through shear thinning bioinks which contribute to the plug flow phenomena. Shear-thinning is common in non-Newtonian fluids, with increases in shear rates resulting in decreases of viscosity.[151] In the plug flow phenomena bioinks behave as fluids only in a thin layer near the extruder walls, whilst the rest of the bioink (the bulk) extrudes as a solid resulting in a more cell-protective flow profile.[118] Rheology is a commonly used method to investigate the flow profile of potential bioinks.

Cell viability

The viability of cells during extrusion is also of key importance when investigating bioprinting methods. Cell viability is often analyzed a few hours or even days after bioprinting. These measurements provide important information for long-term cytocompatibility and proliferation, but not on the cytocompatibility during the actual printing process, such as acute cell damage.[118] Cell death during bioprinting and the curing/crosslinking process is important as the presence of dead or dying cells can affect the overall health and function of surrounding cells.[118,152] Therefore, it is important to evaluate cell viability during the bioprinting and curing/crosslinking process. Live/Dead staining directly after the bioprinting allows the investigation of the ratio of live to dead cells present in the bioprinted construct and to evaluate how "cell friendly" the overall process is.

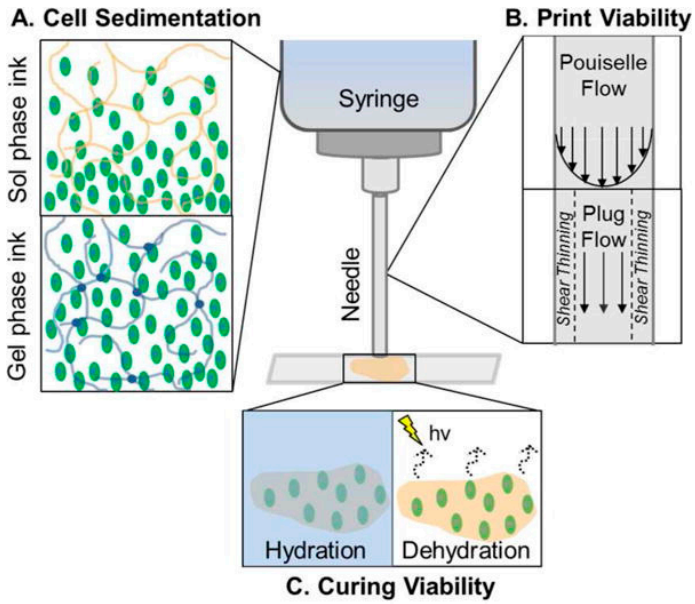

Figure 7 Interactions between cells and the bioink during extrusion based bioprinting

a) Cell sedimentation can lead to non-homogeneous distribution of the cells which ultimately can lead to needle clogging. b) The flow profile of cells experienced when traveling through an extrusion needle, can either be "cell-friendly" or can lead to cell damage and death. c) Depending on the bioink different curing/crosslinking conditions will be needed, which can affect the cell viability through various mechanisms, for example via dehydration or exposure to crosslinking reagents. Figure reproduced from Dubbin et al, 2017 with permission.[118]

Biocompatibility of graft

Tissue engineering and regenerative medicine strategies for organ transplantation offer the potential of custom-designed organs composed of the patients' own cells, potentially avoiding the complications of allogeneic antigens. Ideally, if cells where to be sourced from the transplant recipient, the long-term requirements for immunosuppressive drugs could be circumvented. Thus, in addition to sourcing the cells from the eventual transplant recipient, it is important to identify materials which do not elicit immune responses in the absence of immunosuppression. ECM scaffold materials have been used extensively in tissue engineering and regenerative medicine-based approaches for tissue and organ restoration.[153] The success of these materials in preclinical and clinical applications appears to be attributable, in large part, to their ability to modulate the default mechanisms of wound healing towards a more functional and constructive remodelling outcome. It is increasingly understood that the modulation of the host immune response, in particular, is essential to the formation of new, functional host tissues following scaffold implantation.[154-158]

Immune cell activation and polarization

In general, innate immune cells (neutrophils and macrophages) are the first cells to encounter and respond to implanted biomaterials. Macrophages are differentiated blood monocytes that enter the site of inflammation via the blood stream and which recognize, engulf and degrade debris. Macrophages are key players in both the innate and the adaptive immune response. The immediate cellular response observed following the implantation of an ECM scaffold consists almost exclusively of neutrophils, but there is also a significant mononuclear cell component which replaces the neutrophil response after 72 hours. The presence of these cells, especially mononuclear macrophages, have been shown to be essential to the formation of the type of response that has been observed following the implantation of ECM scaffolds.[155-158] The exact mechanisms by which acellular ECM scaffolds are capable of modulating the default host macrophage response are as yet unknown. However, it is becoming increasingly clear that strategies which promote a transition from an initially type I macrophage (M1-type) response to a more "pro-regenerative" type II macrophage (M2-type) response are better able to promote constructive tissue remodelling and recovery of function than those which promote only an M1 response or lead to a foreign body reaction.[156,158-160]

In addition to eliciting a robust, but constructive, host innate immune response, acellular ECM scaffolds have consistently been shown to evoke a Th2-type T-cell response[161,162], which is generally associated with transplant acceptance.[163] Strategies which elicit more "friendly" Th2 and M2 outcomes will be met with greater success and those which promote a predominantly Th1- and M1-type response can result in chronic inflammation [164,165].

Foreign body response

As mentioned above, chronic inflammation due to biomaterial implantation is most commonly characterized by the presence of activated macrophages which can accumulate up to months after implantation. Accumulation of macrophages for a prolonged time usually leads to granulation tissue formation, foreign body giant cells response, new ECM deposition (fibrosis) and stimulated angiogenesis. Ultimately the biomaterial is encapsulated within a dense layer of collagenous connective tissue to isolate it from the surrounding healthy tissue.

Additionally, calcification is also known to occur in foreign body response and affects many systems in the body. Calcification can occur due to free phosphate and calcium ion increases in the blood which leads to mineral deposition.[166] Problems arising with calcification can occur both naturally in the body, as well as a result of biomaterial implantation including hydrogels.[167] To avoid calcification, hydrogels can be manipulated before implantation, by loading them with metal ions, including iron, aluminum, and magnesium, to prevent mineral deposition.[168,169]

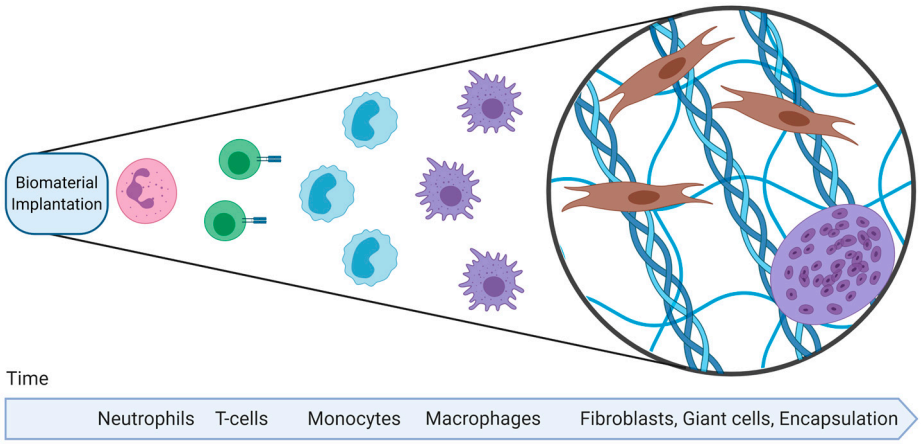

Figure 8 The foreign body response to biomaterial implantation

In the first hours of biomaterial implantation, inflammatory cells including neutrophils and monocyte-derived macrophages infiltrate the wound area in response to the injury. Both M1 and M2 macrophages can be present with M1 secreting pro-inflammatory cytokines and recruiting additional immune cells, while M2 secrete pro-healing and remodeling cytokines. M1 macrophages are more present in foreign body responses. After days or weeks, macrophages can fuse together to form giant cells, and fibroblasts are recruited and collagen deposited, ultimately leading to fibrous capsule formation. Created with BioRender.com

Lessons from skin

Skin regeneration or scar formation is a good starting point to investigate the wound healing response to biomaterial implantations due to its accessibility and previous research undertaken. In skin wound healing, different cell types are recruited which contribute to the timely resolution and closure of wounds. Inflammatory cells infiltrate the wound area and stimulate keratinocyte and fibroblast migration into the wound area. Additionally, neo-angiogenesis assists fibroblast and macrophage based remodeling of fibrin clots and overall strengthening of the tissue by collagen deposition.[170] This collagen layer is remodeled later and it's mechanical properties are adapted to those required by soft tissue by modulating metalloproteinases.[171] The length of the wound healing process with the deposition of ECM affects the overall skin regeneration. Delayed re-epithelialization increases risk of infection. However quick repairs can lead to disorganized ECM deposition and a more pronounced fibrotic response, ultimately leading to scar formation.[171-173]

Vascularization of graft

An intact vasculature is critical for long term functioning of any graft, including successful lung or airway transplantation, and for normal lung function. Blood vessels, of different sizes (in human: microvessels (<1 mm), small vessels (1–

6 mm), and large vessels (>6 mm in diameter)) deliver oxygen and nutrients to tissue and waste away from tissues.[174] Additionally, blood vessels regulate blood flow and permeability, and are important in immunological responses.[174,175] Ideally, bioengineered tissue should have an intact vasculature which should withstand physiological pressures without leakage or aneurysm formation and should not be thrombogenic.[174] An alternative to creating a tissue engineered vasculature, is to stimulate the formation of new vasculature at the transplant site by using pro-angiogenic biomaterials.[8] Recent studies in kidney transplantation have found that rejection is initiated in the donor vasculature[176], indicating that tissue engineered constructs containing vasculature derived from the host may improve transplant outcomes. In line with this finding, recent work has shown that airway transplant success can be improved by first transplanting airway grafts ectopically into the forearm of the recipient to allow pre-vascularization from the eventual recipient.[177]

Aims of the Thesis

The overall scope of this thesis was to bioengineer lung tissue for transplantation with sub-aims listed below.

1. Identify potential bioinks for 3D bioprinting lung tissue (paper I)

2. 3D bioprint functional small airways (paper I)

3. Investigate vascularization and biocompatibility of 3D printed constructs in T-cell immunodeficient mice (paper I) and immunocompetent mice (paper II)

4. Investigate the role of age in cells and scaffolds for regenerative purpose in a skin wound healing model (paper III)

5. Investigate the role of HOPX in IPF alveolar cells to understand the feasibility of using progenitor cells derived from IPF lungs for bioengineering purposes (paper IV)

Summary of Results and Discussion

In paper I, a tissue specific hybrid bioink is developed to 3D bioprint a human airway comprised of primary human epithelial cells and smooth muscle cells, which remains patent over time. The biocompatibility and vascularization of the 3D printed construct is investigated both in immunodeficient (paper I) and immunocompetent mice (paper II). In paper III the use of young matrix and the ability of various subsets of anti- or pro-fibrotic fibroblasts to circumvent scarring in wound healing is investigated. In paper IV the expression of HOPX in alveolar epithelial cells is investigated in diseased IPF lungs.

Generation of a tissue specific hybrid bioink – rECM (paper I)

Recent advances in bioengineering respiratory tissue, including methods to isolate and scale-up epithelial progenitor cells to clinically relevant numbers[178], and innovative surgical techniques to encourage vascularization and graft survival[177,179,180] have brought airway tissue engineering closer to clinical translation. However, scaffolds which can support multiple cell types arranged in their correct anatomical location has not yet been described. Previous attempts to bioengineer airways have mostly focused on the use of decellularising airways to obtain acellular scaffolds for subsequent recellularization. While protocols exist to decellularise airways, including those from human, reattachment and differentiation of primary epithelial cells is challenging. Recently, loss of collagen IV, a major basement membrane protein known to support epithelial cell attachment and differentiation, was reported to be diminished in human airways using conventional decellularization techniques for airways.[181] Decellularization of airways requires aggressive detergents and longer incubation times known to degrade critical ECM components[181,182], which may limit the use of acellular scaffolds. In addition to acellular scaffolds, other techniques have been explored such as models of airways from collagen I[183,184] or surface engineering of materials to enhance cell attachment and vascularization.[185] However, the manufacturing methods tested thus far are not readily amenable to generating branching structures. Furthermore, other ECM components which can support development and maintenance of functional tissue have not been incorporated. In paper I a tissue specific hybrid bioink is developed

which contains a mixture of ECM and proteins derived from decellularized lungs, including both collagen I and IV, components necessary for diverse biological and 3D bioprinting properties to support airway engineering.

Selection of a proper bioink is a critical first step in establishing 3D bioprinting applications for specific tissues. ECM solutions derived from pepsin-digested decellularized tissues, including lung, have been previously shown to form hydrogels when incubated at 37°C due to spontaneous self-assembly of ECM components such as collagens.[186,187] ECM solutions from tissues other than lung have been previously used as bioinks in 3D bioprinting applications.[144,188] Therefore, the ability of lung ECM solutions derived from pepsin-digested decellularized mouse lungs were first tested to form hydrogels. Despite the retention of collagens (Figure 9b), including collagen I and IV (Figure 9c,d) at sizes known to be critical for hydrogel formation[187], hydrogels did not spontaneously form at conditions permissible for gelation of purified collagen I (Figure 9a).

In order to obtain consistent gelation suitable for 3D bioprinting, the potential of combining the (murine on human) ECM solution with another polymer commonly used in 3D bioprinting, alginate[189], was tested. Alginate can be quickly crosslinked with the addition of divalent cations to form hydrogels.[190,191] Therefore, the addition of alginate to lung ECM solutions could enable hydrogel formation. Upon Ca^{2+} addition, hydrogels rapidly formed translucent hybrid bioinks, in this thesis named as reinforced extracellular matrix bioinks (rECM). The rECM hydrogels were determined to form well-mixed, phase separated hydrogels instead of interpenetrating networks.[192] As phase separated materials can be mechanically inferior to single phase materials, the mechanical properties at the bulk hydrogel level were tested. The addition of ECM components in rECM hydrogels resulted in increased mechanical stability under shear stress compared to alginate hydrogels at the same weight percentage (Figure 9e).

The presence of lung derived ECM in rECM bioinks addresses one of the major current limitations to most commonly used bioinks: the lack of native, tissue-specific ECM-like components.[143] These components are critical for cells to recognize and interact with their microenvironment to develop functional tissues. ECM solutions have been derived from a variety of different tissues and organs, therefore the current hybrid approach could be widely adapted. By using hybrid materials as described here, the biological components of the native tissue microenvironment are retained and can be combined with other materials with properties advantageous for 3D printing and final tissue maturation.

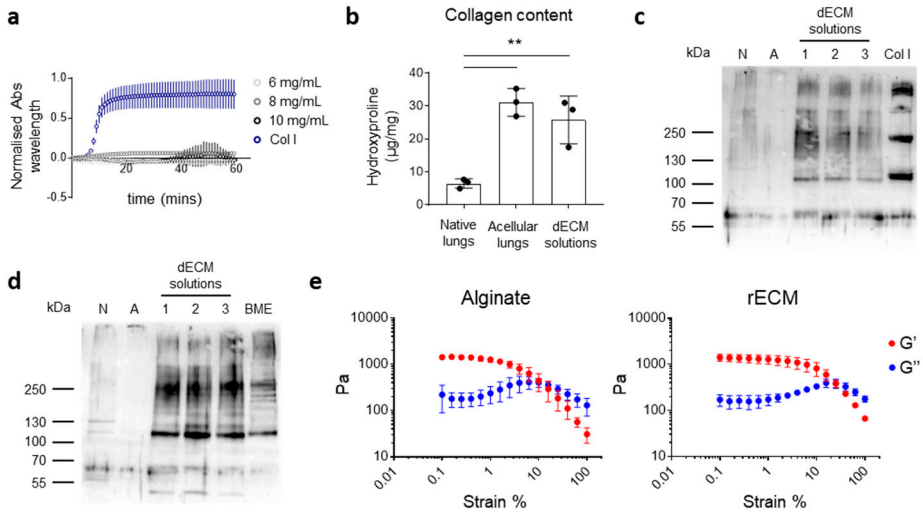

Figure 9 Mouse dECM solutions do not spontaneously gelate despite retention of collagens and rECM hydrogels are more mechanically stable than alginate hydrogels.

a) Gelation kinetics of ECM solutions at different concentrations (6, 8 and 10 mg mL-1) compared to rat tail type I collagen (3.7 mg mL-1). b) Hydroxyproline content in native lungs, acellular lungs, and ECM solutions (n=3/group). c) Collagen I Western blot showing collagen I content in native (N), acellular mice lungs (A), 10 mg mL-1 ECM solutions (1, 2 and 3) and rat tail type I collagen (Col I). d) Collagen IV Western blot showing collagen IV content in native (N), acellular mice lungs (A), 10 mg mL-1 ECM solutions (1, 2 and 3) and basement membrane extract (BME). e) Mean curves of the moduli G' and G'' as a function of the strain of alginate and rECM hydrogels (n=3/group). **p < 0.01. Figure and text taken from De Santis et al, 2020 with permission.[193]

rECM bioinks are compatible with bioprinting (paper I)

rECM bioinks are shear thinning and resist cell sedimentation

To confirm that rECM solutions did not result in bioink properties incompatible with printing flow (e.g. shear thickening)[194], oscillatory rheometry was used to investigate the flow profile (Figure 10a). The addition of ECM in rECM bioinks resulted in shear thinning bioinks, which is beneficial for 3D bioprinting. In addition to evaluating shear thinning behaviours, the resistance to cell sedimentation of rECM bioinks was investigated. Bioprinting of many clinically relevant products will take several hours[195], therefore bioinks which prevent cell sedimentation are advantageous for mitigating clogging of the print head and for generating large constructs with homogenously distributed cells.[194] A recently established cell sedimentation assay[194] was used to show that the presence of alginate in bioinks significantly reduced the cell sedimentation abilities (quantified into sedimentation coefficients (δ)) as compared to ECM solutions and cell culture media (Figure

10b,c). Therefore, both the alginate and the ECM components in rECM bioinks are required to simultaneously fulfil several optimum criteria for 3D bioprinting.

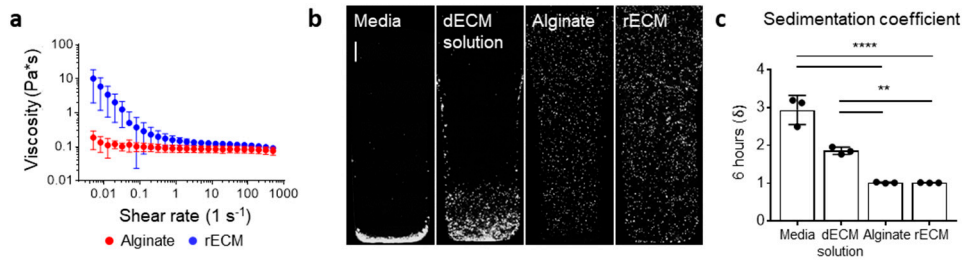

Figure 10 rECM bioinks are shear thinning and resist cell sedimentation

a) Rheometry of alginate and rECM solutions b) Cell sedimentation confocal images and (c) calculated sedimentation coefficient (δ) of A549 cells in DMEM-F12 cell culture media, alginate, mouse-derived dECM and rECM solution for 6 h (n=3/group). Scale bar, 500 µm. **p < 0.01, ****p < 0.0001. Figure and text taken from De Santis et al, 2020 with permission.[193]

rECM bioinks and the bioprinting process is cytocompatible

rECM bioinks were shown to improve cell viability of cell lines and human primary cells over prolonged periods of times. Cells survived the FRESH printing process in both alginate and hybrid hydrogels, with noticeable increases in cell numbers over seven days, indicating cytocompatibility of the process. Interestingly, human lung epithelial cells (A549) had increased metabolic activity when 3D bioprinted in hybrid bioinks as compared to alginate (Figure 11a). However, no changes in metabolic activity were observed in this same cell type when hydrogels were formed using manual extrusion through a pipette (i.e. *in vitro*), indicating that the hybrid bioink protects cells during 3D bioprinting. To better understand the difference in observed metabolic activity, computational fluid dynamics was used to investigate whether the hybrid and alginate solutions have different fluid shear stress profiles leading to cell damage during the 3D printing process. The average shear stress profiles for the two bioinks is highly similar (Figure 11b). This indicates that the difference observed in metabolic activity post-printing does not originate from the bulk fluid properties but is likely due to the presence of biologically active factors within the ECM solution.

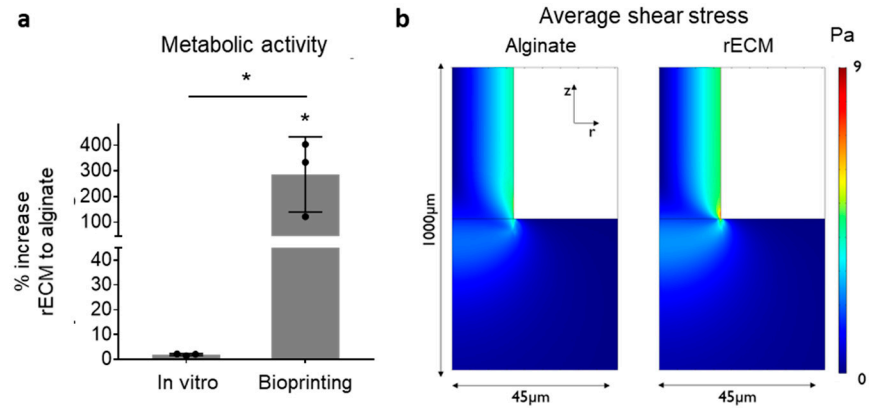

Figure 11 rECM bioinks and bioprinting process support cell viability

a) Metabolic activity (WST-1) on day 7 of seeded *(in vitro*) and bioprinted A549 cells in hydrogels. b) Average shear stress profiles of bioinks. *p < 0.05. Figure and text taken from De Santis et al, 2020 with permission.[193]

rECM bioinks promote progenitor differentiation into mature epithelial cells (paper I)

In comparison to alginate, bronchial epithelial cells grown at air liquid interface (ALI) on rECM hydrogels exhibited increased expression of a range of phenotypic markers found in the adult human airway epithelium (e.g. goblet cells (MUC5AC and MUC5B), ciliated cells (FOXJ1) and club cells (CC10) both on protein and the RNA level (Figure 12a,c). Bronchial epithelial cells grown on alginate and rECM hydrogels developed into ciliated cells as observed via scanning electron microscopy (Figure 12b). However, when further investigating the ciliated cells via transmission electron microscopy, differences in the ciliary ultrastructures were observed. Compound cilia were present in HBECS seeded on alginate but not on rECM hydrogels (Figure 12d,e). Compound cilia are acquired ultrastructural ciliary defects which are present in acquired ciliary dyskinesia.[196,197] However, correlating specific acquired ultrastructural defects, with loss of ciliary function is difficult [198] as normal ciliary function has been observed in patients with compound cilia. To investigate more in depth differences in ciliary function and movement, high resolution and high speed videos with or without fluorescent beads, could be used.

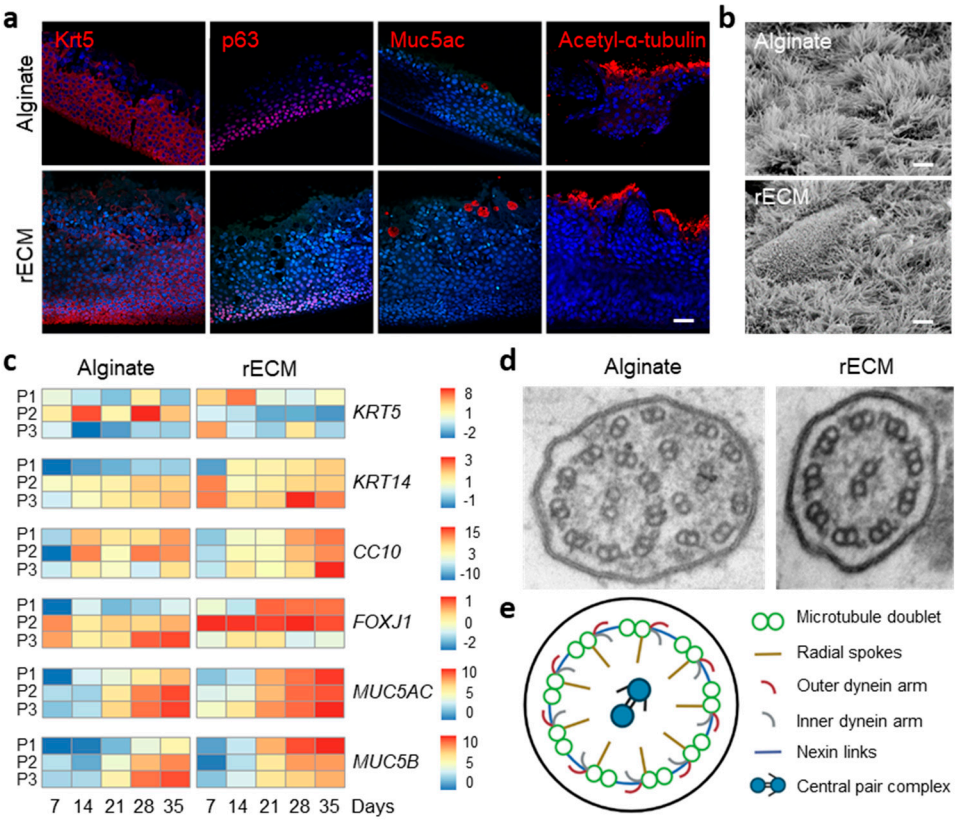

Figure 12 rECM bioinks promote differentiation of human bronchial epithelial cells into adult human airway cells

a) Changes in gene expression of HBECs seeded on top of alginate and rECM hydrogels and lifted to ALI on day 7 showing the fold change compared to day 0 of differentiation genes on day 7, 14, 21, 28 and 35 (increase in red and decrease in blue) (n= 3 patients/group (P1, P2 and P3)). b) Transmission electron microscopy images of normal cilia on rECM and compound cilia on alginate (n= 3 patients/group (P1, P2 and P3)). c) Diagram showing features of cilia ultrastructure (created with BioRender.com). Panel a-c and text taken from De Santis et al, 2020 with permission.[193]

rECM bioinks are biocompatible and pro-angiogenic in immunodeficient mice (paper I)

As 3D bioprinting moves towards printing full-scale tissues and organs, the ability of bioinks to promote vascularisation is key. Intact vasculature is critical for successful lung and airway transplantation[174] and recent studies in kidney transplantation have found that rejection is initiated in the donor vasculature[176], indicating that tissue engineered constructs containing vasculature derived from the host may improve transplant outcomes. In line with this finding, recent work has shown that airway transplant success can be improved by first transplanting airway

grafts ectopically into the forearm of the recipient to allow pre-vascularization from the eventual recipient.[177] Therefore, 3D printed constructs that promote vascularisation are ideal to support short and long term graft survival. rECM bioinks were shown to be pro-angiogenic in a CAM assay and in an immunodeficient T-cell deficient *FoxN1* KO mouse model to mimic clinical immunosuppression in transplant patients (Figure 13).[193]

Moreover, rECM bioinks were able to regulate the immune response upon implantation, reducing the pro-inflammatory response elicited by some forms of alginate. ECM has been previously shown to promote tissue repair and constructive remodelling and has been used to accelerate wound repair[199,200] and mitigate acute lung injury.[201] However, this is the first time that ECM derived components of a 3D bioprinted hybrid material have been shown to suppress the foreign body response elicited by other materials of the hybrid. This opens up new possibilities for combining ECM solutions with other polymers which lack biologically inductive properties but can help standardise properties such as gelation time and reduce the amounts of costly ECM-derived materials.

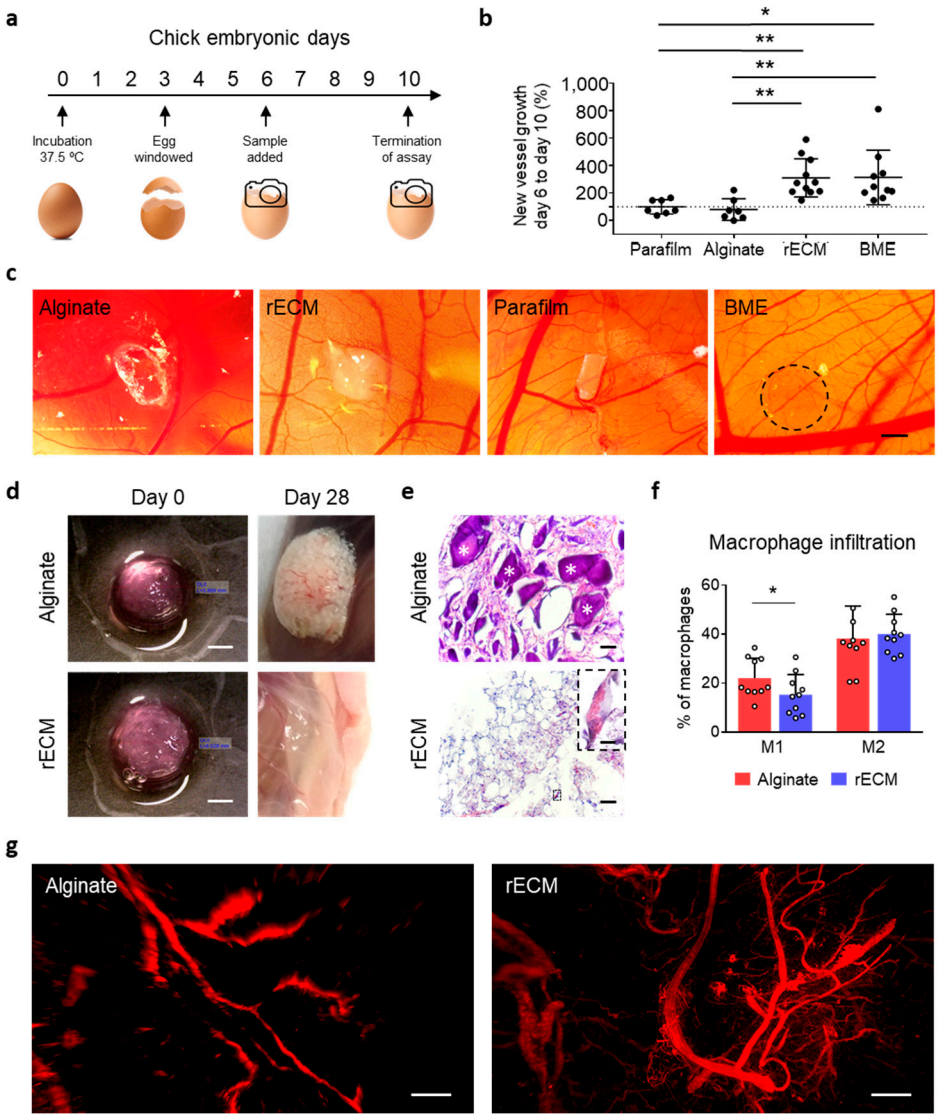

Figure 13 Biocompatibility and angiogenic potential of rECM hydrogels.

a) Overview of CAM procedure. b) Changes in blood vessel formation, i.e. blood vessels on day 10 compared to day 6 and normalized to parafilm (100%) for each sample group. (n=7-10/group). c) Images of BME (positive control), parafilm (negative control), rECM and alginate hydrogels on CAMs on day 10. Scale bar, 1 mm. d) 3D printed alginate and rECM hydrogels in disk shape before subcutaneous implantation and when explanted on day 28. Scale bars, 2 mm. e) H&E staining of subcutaneously implanted alginate and rECM hydrogels after 28 days. White asterisks * indicate large, non-proteinaceous debris. Inset showing red blood cells in the inner lumen of a blood vessel. Scale bars, 50 µm and 10 µm (inner panel). f) Macrophage infiltration (defined by CD45+, CD11b+ and F4/80+) in implanted alginate and rECM hydrogels on day 7 (n=10 animals/group). g) Light sheet microscopy images (maximum intensity projections) of explanted alginate and rECM hydrogels (day 28) after optical clearing, showing blood vessel infiltration visualized by autofluorescence (Ex/Em: 480/520 nm). Scale bars, 250 µm. *p < 0.05, **p < 0.01. Figure and text taken from De Santis et al, 2020 with permission.[193]

3D bioprinted small airways using human derived rECM bioinks (paper I)

In order to establish a translationally relevant bioprinting work flow, human rECM bioinks which have similar attributes to murine hybrid bioinks, were used to 3D bioprint subsegmental bronchi. Subsegmental bronchi are around 4 mm in diameter and composed of an outer smooth muscle layer and an inner epithelial layer.[202] To bioprint two different primary cell types, a custom-built dual extrusion system was used. Subsegmental bronchi were generated by 3D bioprinting hollow tubes consisting of three concentric print layers: an inner layer of HBECs at a nominal diameter of 4 mm and two sequential layers of primary human lung smooth muscle cells (HLSMCs) at nominal diameters of 5 and 6mm, mimicking the anatomical location of the two cell types in human airways (Figure 14a). The dual extrusion system produced hollow tubes at high fidelity to the dimensions of the 3D digital model with distinct, but connected cell layers. The airspaces of 3D bioprinted human airways remained open during 20 days of ALI *ex vivo* culture, suggesting that constructs are stable for at least 28 days (Figure 14b). Furthermore, cells remained within their respective layers of the engineered airways and HBECs differentiated into ciliated cells (positive for Acetylated α-tubulin) (Figure 14c). Taken together, human hybrid bioinks supported the formation of a 3D bioprinted human airway comprised of regionally specified primary human lung cells which can differentiate towards mature human airway epithelial cell types.

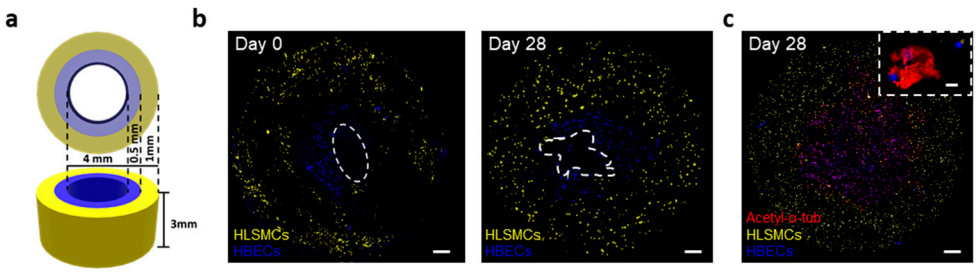

Figure 14 rECM bioinks for 3D bioprinting small airways

a) 3D rendering of bioprinted airways. b) 3D bioprinted airway with human lung smooth muscle cells (HLSMCs) in yellow in the outer perimeter and human bronchial epithelial cells (HBECs) in blue in the lumen on day 0 and on day 28 (n=3 patients/group). Dotted white lines indicate the inner lumen. Scale bars, 500 µm. c) 3D bioprinted airway with acetylated-α-tubulin staining in red on day 28 (n=3 patients/group). Inner lumen appears closed due to a processing artefact. Scale bar, 500 µm (lower) and 25 µm (upper). Figure and text taken from De Santis et al, 2020 with permission.[193]

rECM bioinks are biocompatible and pro-angiogenic in immunocompetent mice (paper II)

Tissue engineering and regenerative medicine strategies for organ transplantation offer the potential of custom-designed organs composed of the patients' own cells, potentially avoiding the complications of allogeneic antigens. Ideally, if cells where to be sourced from the transplant recipient, the long-term requirements for immunosuppressive drugs could be circumvented. Thus, in addition to sourcing the cells from the eventual transplant recipient, it is important to identify materials which do not elicit immune responses in the absence of immunosuppression. The use of immunocompetent animal models is an ideal model to screen immunogenicity of candidate biomaterials as the host response to the implanted material will dictate long-term success or failure.[203] In paper II the biocompatibility of 3D FRESH printed rECM hydrogels from alginate and lung derived extracellular matrix in immunocompetent mice was investigated after 7 and 28 days.

rECM hydrogels support the formation of an intact vascular network throughout the full thickness of the graft, comprised of both large and small size blood vessels (Figure 15). On the other hand, vasculature was less developed in the alginate hydrogel. Both alginate and rECM hydrogels integrated well in the surrounding tissue exhibiting a remodelling phenotype. Taken together, 3D printed rECM constructs do not illicit negative immune responses when transplanted into immunocompetent mice, integrate well in the surrounding tissue without evidence of a foreign body response, are pro-angiogenic and support *de novo* vasculature.

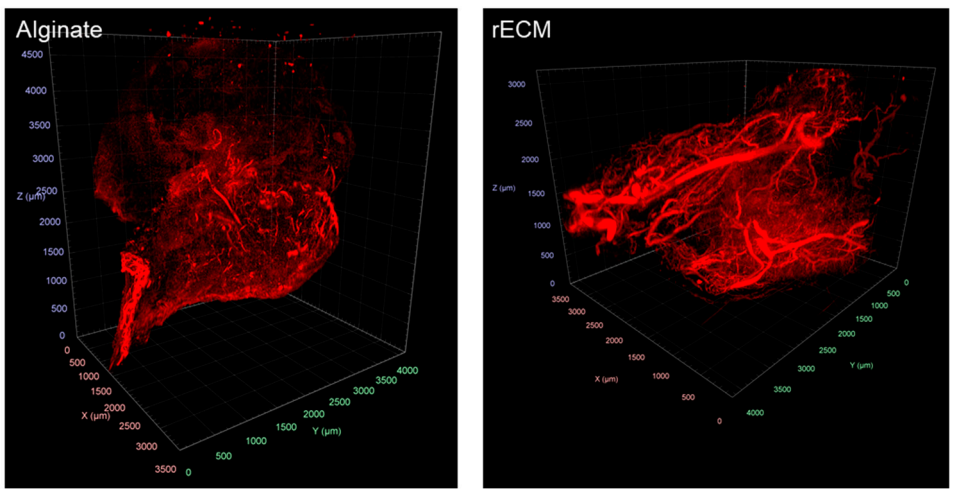

Figure 15 Vascularization of rECM hydrogels in immunocompetent mice.

Light sheet microscopy images (maximum intensity projections) of explanted alginate and rECM hydrogels (day 28) after optical clearing, showing blood vessel infiltration visualized by autofluorescence (Ex/Em: 480/520 nm)

Cell and scaffold age determine regenerative capacity of skin (paper III)

Acellular tissue scaffolds retain bioactive properties and some tissue specificity,[77,89] with studies showing aged and diseased scaffolds driving the acquisition of deranged cellular phenotypes in cells from normal patients.[6,80,81,93,204,205] During fetal development, mammalian back-skin changes its response to injury, from scarless regeneration to skin scarring. Thus, the role of cell and scaffold age on the regenerative capacity of skin was investigated. Dermal development and regeneration is driven by engrailed 1-history-naive (ENFs) and engrailed 1-history-positive fibroblasts (EPFs). ENFs are present at high numbers in the embryonic stage with numbers subsequently declining over time.[59] EPFs on the contrary, are not present in early embryonic stages but start to populate the neck of the embryo at E10.5 and expand to posterior regions over time. At birth the majority of fibroblast (around 70%) are EPFs. EPFs are shown to be the major wound healing fibroblast population in adults and drive the scarring process. When ENFs are transplanted into the wound, the scarring severity is dramatically reduced (Figure 16).

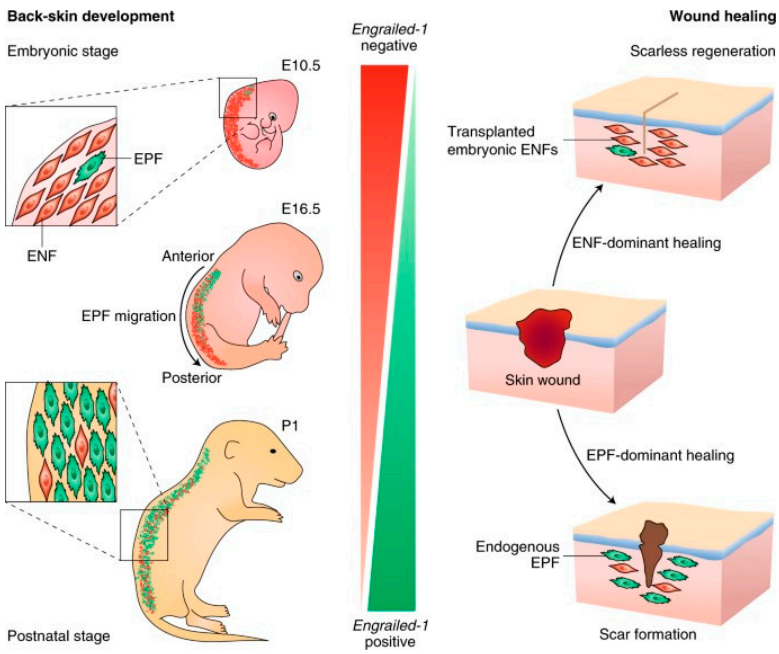

Figure 16 Role of EPFs and ENFs in back skin development and scar formation during wound healing

(Left) Lineage transition from ENF to EPF cells. At early embryonic stages, the majority of back skin fibroblasts are ENFs. Over time, ENF numbers decrease with EPF number increasing and expanding to posterior regions. At birth the majority of fibroblasts are EPFs. (Right) EPF-dominant healing results in scar formation. An improved scar outcome is observed when transplanting ENFs or acellular ECM derived from P5 back skin. Figure and modified text taken from Yokoyama & Rafii, 2018 with permission.[172]

In order to investigate whether the ENF-generated ECM itself could promote a more regenerative outcome, acellular back-skin from P5 WT mice was transplanted into the skin wounds (Figure 17a). Fibroblasts present at the border between the wound and the matrix were found to be activated with elongated cytoplasm and α-SMA positivity, as was the case for fibroblasts in control wounds (Figure 17b,c,e,f). This was not the case for fibroblasts present in the transplanted acellular matrix in the wound area (on day 10) which presented an inactive phenotype as shown by their α-SMA negativity and inactive morphology (round cytoplasm) (Figure 17d,g). Thus, restoration of a 'healthy' dermal lattice can be stimulated by either transplanting ENFs which expand the existing pool of resident ENFs to sculpt a provisional matrix, or alternatively, by transplanting an acellular dermal lattice derived from a young mouse, which prevents EPFs from generating a pathological scar.[59] These approaches could be translated clinically providing therapeutic possibilities for different dermal pathologies.

The results presented here are supported by a recent study indicating that scaffolds derived from early post-natal human lungs support better re-epithelialisation as compared to those derived from adult lungs.[206] Despite the fact that human scaffolds from aged patients are somewhat readily available, they are therefore not presently considered as ideal sources for lung tissue engineering approaches.

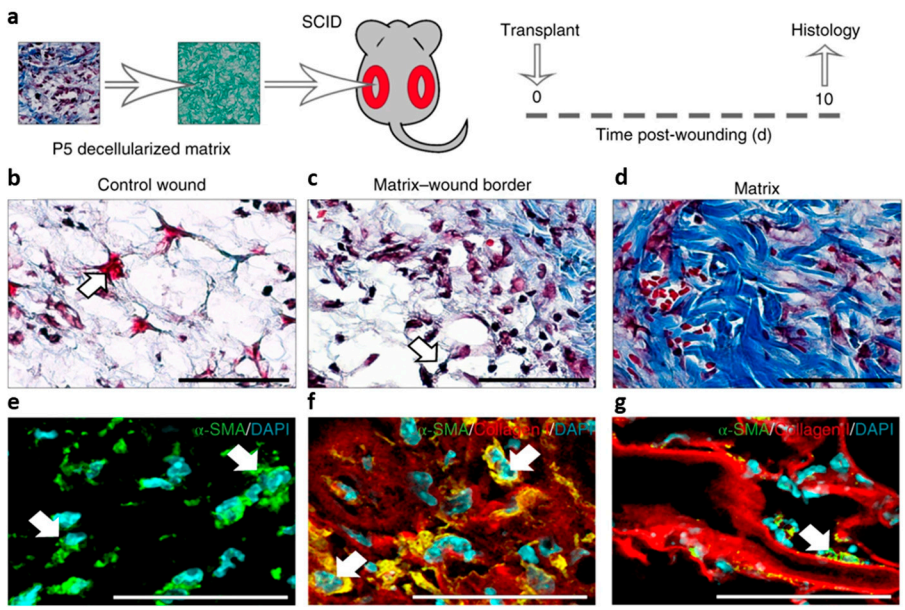

Figure 17 Role of young acellular matrix in scar formation during wound healing

(a) Acellular matrix transplantation experiment schematic. Back-skin explants from P5 WT mice were decellularized and transplanted into fresh wounds of adult immunodeficient mice with tissue collection after 10 days (b-g), Masson's trichrome-stained (b-d) or α-SMA-stained and collagen I-stained (e-g) control wounds (b,e), the border between the transplanted matrix and the wound (c,f) or within the transplanted matrix (d,g). Scale bars, 50 μm. Figure and modified text taken from Jiang et al, 2018 with permission.[59]

Progenitor cells can be deranged in diseased lungs (paper IV)

As mentioned previously, ideally, autologous cells from the patient would be used for recellularising lung scaffolds in order to minimise post-transplantation immune complications and the need for immunosuppressive medications. Induced pluripotent stem cells (IPSC) or progenitor cell populations derived from the patient could be used to direct differentiation into the different cell types found in the adult lung. Progenitor cell populations can be controlled more easily than IPSCs, with lower risk of tumour formation. However, progenitor cells can be deranged in diseased lungs such as for example IPF. The mechanisms of injury and repair that occur in alveolar epithelial cells influence the progression of lung diseases such as IPF. Homeobox only protein x (HOPX) contributes to the formation of distal lung during development and is known to regenerate alveoli after trauma such as pneumonectomy. In healthy adult lungs, ATI cells express HOPX which can give rise to both ATI and ATII cells. The function of HOPX-expressing cells in adult fibrotic lung diseases, instead is not fully known. To better understand this the presence of HOPX+ cells was investigated in healthy and IPF human lungs and in a model of pulmonary fibrosis, the bleomycin murine model (Figure 18). HOPX expression is decreased overall in IPF lungs (Figure 18b) and significantly correlates to lung function decline and disease progression of IPF.[20] However, interestingly, HOPX was found to be upregulated in bleomycin treated mice (Figure 18a). Thus, it is postulated that HOPX is upregulated during alveolar injury and the lung repair process, whilst the lower expression of HOPX observed in end stage IPF lungs could contribute to the regenerative failure of IPF lungs. Thus, progenitor cells derived from diseased lungs are likely not an appropriate source to generate healthy tissue. From this it is clear that to generate a healthy tissue or organ, it is critical to find the appropriate scaffold and cell type.

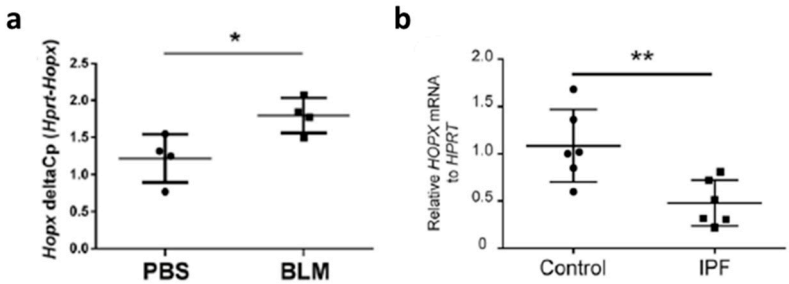

Figure 18 HOPX expression in healthy and IPF lungs

(a) HOPX mRNA in PBS and bleomycin instilled mice. (b) HOPX mRNA from whole lung homogenate of control and IPF lungs. *p < 0.05, **p < 0.01. Figure taken from Ota et al, 2018 with permission.[20]

Conclusion and Future Perspectives

Next generation lung bioengineering approaches attempt to combine cells with natural, synthetic or hybrid matrices and grow the bioengineering tissue *ex vivo* before hypothetical transplantation. To generate healthy lung tissue, it is critical to find the appropriate scaffold and cell type.

In **paper I** a tissue specific rECM bioink was developed and used to bioprint for the first time a human airway comprised out of primary smooth muscle and bronchial epithelial cells which differentiate into cells present in the adult airway. The bioprinted human airway remains patent over time and rECM constructs implanted into T-cell immunodeficient mice are biocompatible and pro-angiogenic. rECM bioinks could be used to 3D bioprint respiratory tissue not only for transplantation purposes but also for applications such as *in vitro* drug screens and disease modeling. Major questions remain such as whether the 3D bioprinted airways will maintain airway patency *in vivo*, the extent of vascular integration upon orthotropic transplantation, and whether cells will retain their differentiation profile when transplanted. The bioink will also need to be modified depending on the size of the airway in order to mimic the correct mechanical properties. One aspect not investigated in this study is the use of a bioreactor to mature the cells into their differentiated state. Bioreactors will likely be required to engineer larger airway segments and this will be critical for future studies.

In **paper II** the biocompatibility and vascularization potential of bioprinted rECM constructs is investigated in immunocompetent mice. rECM hydrogels support the formation of an intact vascular network throughout the full thickness of the graft, comprised of both large and small size blood vessels in the presence of a fully competent immune system and integrate well in the surrounding tissue. Other aspects to consider are the peripheral immune response to better understand the adaptive/innate immune response to the implanted constructs and the presence of myeloid angiogenic cells (MACs) which significantly promote vascular repair *in vivo*.[207] It would be interesting to see how this differs between T-cell immunodeficient and immunocompetent mice.

In **paper III** the role of cell and scaffold age on the regenerative capacity of skin is investigated in the wound healing response. Fibroblastic lineages evolve over time with fibroblasts present in early embryonic stages (ENFs) and their resulting matrices promoting scarless regeneration. Human scaffolds from aged patients are therefore, not the ideal sources for lung tissue engineering approaches. Importantly, one aspect left to investigate is the recruitment of inflammatory cells in scarless

wound healing by ENFs or transplanted acellular matrices. In addition to fibroblasts and endothelial cells, monocyte infiltration could likely play a role in the extent of scarless healing. Recruitment of macrophages is crucial for successful regeneration, yet their role in chronic wounds is not fully understood.[208] Macrophages mediate the inflammatory response by secreting cytokines and chemokines which contribute to the closure of the wound. Thus, it is important to better understand the interaction between specific fibroblastic lineages, such as ENFs, and different types of monocytes to hopefully achieve a more efficient wound healing.

In **paper IV** expression of HOPX in IPF lungs was investigated to assess the feasibility of using progenitor cells derived from diseased lungs in bioengineering approaches for eventual transplantation. HOPX was found to contribute to the alveolar repair process in fibrotic lung diseases. However, end-stage IPF lung alveolar epithelium does not regenerate, likely due to loss of HOPX. Thus, HOPX could be used as a potential indicator of fibrosis progression. Aberrant expression of regenerative progenitor cell markers postulates that progenitor cells derived from diseased lungs are likely not the best candidates for lung tissue engineering approaches.

Materials and Methods

Mouse and Human tissue

Paper I

Human lung tissue was obtained from discarded surgical waste from donor lungs following lung transplantation. The study was approved by the local Ethics Committee for Research in Lund, Sweden (Dnr 2017/396). Seven human lungs were used in the studies, four for ECM solutions with an average age of the patients of 36 years, with three females and one male.

Paper I and II

8-14 week-old male and female wildtype C57BL/6J were obtained by Janvier and Charles River and housed in individually ventilated cages in rooms with constant humidity and temperature with 12-hours light cycle and access to water and food ad libitum. All animal studies were performed under the strict regulation of the Swedish board of agriculture and approved by the Lund University Ethical committee (Approval numbers: 5.8.18/12637/2017, M 152-14 and M 57-16).

Paper III and IV

All mouse strains (C57BL/6J (WT), En1Cre, ActinCre-ER, R26VT2/GK3, R26mTmG and $Rag2^{-/-}$) were obtained from Jackson laboratories, Charles River, or generated at the Stanford University Research Animal Facility, and were housed at the Helmholtz Center Animal Facility. The rooms were maintained at constant temperature and humidity with a 12-hour light cycle. Animals were allowed food and water ad libitum. All animal experiments were reviewed and approved by the Government of Upper Bavaria and registered under the project 55.2-1-54-2532-61-2016 and project 55.2-1-54-2532-88-12 and conducted under strict governmental and international guidelines.

Decellularization

Lungs

Native lungs were decellularized using a combination of detergent and enzyme solutions previously developed.[6,79] Mouse lungs were harvested from wildtype C57BL/6J mice with the heart and trachea *en bloc*. Decellularization solutions were perfused both through the trachea (airways) and the heart right ventricle (vasculature) (Table 2). For mouse lungs, rinses using a total of 30 mL solution were undertaken (15 mL through the trachea and 15 mL through the heart). For the decellularization solutions a total of 6 mL was used (3 mL through the trachea and 3 mL through the heart). For human lungs, volumes were adapted to the size of each lung to ensure maximal filling with each decellularization reagent at least once and an extra sterilization step was undertaken with perfusion of 0.1% peracetic acid (Sigma) in 4% ethanol solution before storage. Acellular lungs were stored at 4°C in PBS supplemented with antibiotics until further use.

Table 2. Decellularization method for human and murine lungs.

Day	Reagent	Amount	Time	Temperature	Company
1	De-ionized (DI) water + 500 IU/mL Penicillin and 500 ug/mL Streptomycin (5X pen/strep)	30 mL	Rinse	25°C	VWR International AB
1	0.1% Triton-X	6 mL rinse and 20 mL incubation	Rinse and 24-hour incubation	4°C	Sigma
2	DI water + 5X pen/strep	30 mL	Rinse	25°C	VWR International AB
2	2% SDC	6 mL rinse and 20 mL incubation	Rinse and 24-hour incubation	4°C	Sigma
3	DI water + 5X pen/strep	30 mL	Rinse	25°C	VWR International AB
3	1M NaCl	6 mL rinse and 20 mL incubation	Rinse and 1-hour incubation	25°C	Sigma

3	DI water + 5X pen/strep	30 mL	Rinse	25°C	VWR International AB
3	30 µg/mL porcine pancreatic Dnase + 2 mM $CaCl_2$ + 1.3 mM $MgSO_4$	6 mL rinse and 20 mL incubation	Rinse and 1-hour incubation	25°C	Sigma
3	5X pen/strep + 50 mg/L gentamicin + 2.5 ug/mL Amphotericin B in 1X PBS solution	30 mL rinse and 20 mL incubation	Rinse and incubation	4°C	VWR International AB

Validation methods for decellularization

Acellular lungs were routinely validated using the guidelines set forth by Crapo et al. which include absence of visible cellular or nuclear material on histological examination, less than 50 ng dsDNA per 1 mg of dry weight of the ECM scaffold, and remnant DNA shorter than 200 bp.[62] In this work we used H&E and Masson's Trichrome stainings and a Quant-iT™ PicoGreen™ dsDNA Assay (Invitrogen™) to validate decellularization (n=3-4 animals or patients). The retention of proteins in acellular lungs was further quantified using a Hydroxyproline Assay Kit for collagen (Sigma Aldrich) and western blot for collagen I and collagen IV, the most abundant collagens found in lung tissue.

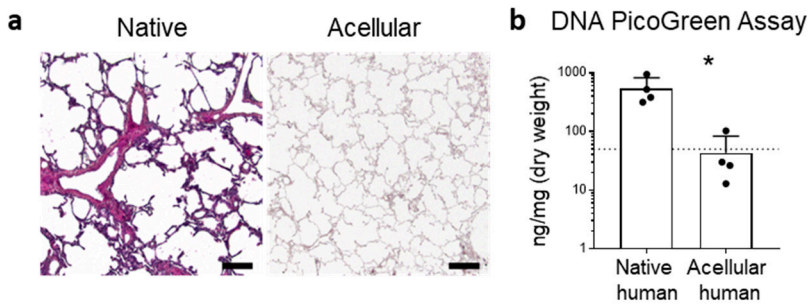

Figure 19 Decellularized human lungs

a) Representative H&E stainings of native and acellular human lungs showing the absence of visible cellular or nuclear material. Scale bars, 200 µm. b) DNA quantification in native and acellular human lungs using a PicoGreen assay. The dotted line marks the benchmark criteria of <50ng DNA/mg dry tissue weight for effective tissue decellularization (n=4/group). Figure and text taken from De Santis et al, 2020 with permission.[193]

Skin

The dorsal skin was surgically removed from C57BL/6J mice (age P5) and subjected to decellularization similar to above. Briefly, the hair from the skin tissue was removed using a hair removal solution and the skin tissue was then incubated sequentially first with distilled water containing 0.1% Triton X-100 and 5× pen/strep at 4 °C for 24 hours, then with distilled water containing 2% SDC at 4 °C for 24 hours, distilled water containing 1 M NaCl, 5× pen/strep at room temperature for 1 hour, and finally, distilled water containing 30 µg ml–1 porcine pancreatic DNase, 1.3 mM MgSO4, 2 mM CaCl2 and 5× pen/strep at room temperature for 1 hour. The skin tissue in incubation solutions was left to incubate on a shaker. The decellularized skin was stored in PBS supplemented with antibiotics at 4 °C until transplantation.

Transplantation of decellularized skin

Two 5-mm diameter full-thickness excisional wounds were created on the dorsal back of each recipient Rag2$^{-/-}$ immunodeficient mouse. A 5-mm diameter biopsy of acellular WT mouse skin was transplanted to the recipient's wound with silicone elastomer super glue (Kwik-Sil Adhesive, World Precision Instruments). Wounds without acellular skin transplants served as control. Wounds were covered with a 12-mm diameter silicone sheet (Grace Bio-Labs), fixed with 5 sutures, and transparent dressing (3 M Tegaderm Film). After 10 days the wounded areas were harvested and processed for histology. Text modified from Jiang et al.[59]

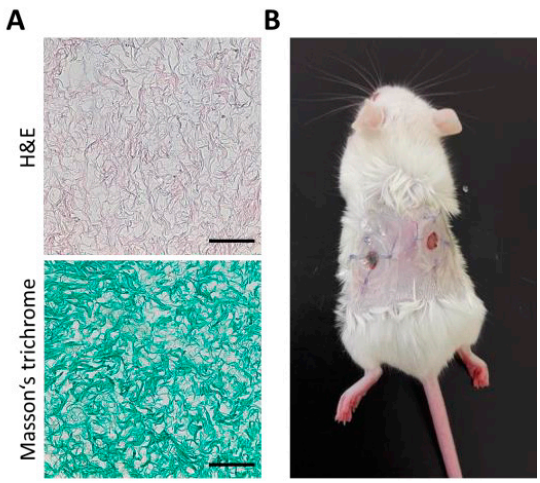

Figure 20 Decellularization of murine skin.

a) Representative H&E and Masson's Trichrome stainings of acellular murine skin showing the absence of visible cellular or nuclear material and the retention of collagen. Scale bars, 100 µm. b) Image of recipient SCID mice after wounding and transplantation.

In vitro cell culture for cell lines and hydrogels:

Murine and human lung epithelial cells (MLE12 and A549), murine brain endothelial cells (bEnd.3) and human lung smooth muscle cells (HLSMCs) were purchased from ATCC® (CRL-2110, CCL-185, CRL-2299 and PCS-130-010). Cell lines were cultured in DMEM/F12 medium (Gibco) supplemented with 10% FBS, 100 mg L-1 streptomycin, and 100 U mL-1 penicillin. Primary HLSMCs were cultured in vascular cell basal medium supplemented with vascular smooth muscle growth kit (ATCC®). Cells were grown using standard cell culture conditions at 37 °C, 5% CO_2 until 70–80% confluency and then mixed with pre-gel solutions (1 million cells/mL) to form bioinks. Bioinks were pipetted onto 24 or 96 well plates and crosslinked using 50 mM $CaCl_2$ solution. Excess $CaCl_2$ solution was removed and DMEM/F12 medium added. Media was changed every other day. Text modified from De Santis et al.[193]

Cell proliferation staining

Live staining was performed using the Cell Proliferation Staining Reagent Deep Red or Blue Fluorescence Cytopainter (abcam) following the manufacturer's instructions. Briefly, cells were incubated with the dye solution for 30 minutes, washed with PBS three times and then mixed in bioinks prior to crosslinking. Z-stack images were acquired using confocal microscopy (n=3/condition). Text taken from De Santis et al.[193]

Wst-1 assay

Metabolic activity was performed using Wst-1 (ab155902, Abcam, Cambridge, UK) following the manufacturer's instructions. Briefly, 20 µL of reconstituted Wst-1 reagent was added in 180 µL of media to 96 well plates containing cell laden hydrogels and incubated for 30 minutes at 37 °C, 5% CO2. The absorbance was then measured at 490 nm using a PHERAstar FS spectrophotometer (BMG LABTECH). Text taken from De Santis et al.[193]

Rheometry

Rheological measurements were carried out by using a stress-controlled rotational rheometer (MCR302, Anton Paar) equipped with different geometries depending on the measured samples. Pre-hydrogel solutions (~1 ml) were loaded between a cone and plate geometry (CP50-1) of 50 mm diameter and 1° angle for measuring their flow curves. Hydrogels were loaded between two parallel plates (PP15) of 15 mm

diameter and under a constant normal force and gap size, both ranging from 0.04 to 0.5 N and from 0.5 to 0.8 mm, depending on the samples, respectively.[209] Amplitude strain sweep tests were performed at a constant frequency of 10 rad/s and strain ranging from 0.1% to 100%.[210,211] All the measurements were performed at 25 °C (n=3 batches/condition). Text taken from De Santis et al.[193]

Cell sedimentation assay

Cell sedimentation within the different bioinks was assessed using a previously published assay.[118] A549 cells were labeled with Cell Proliferation Staining Reagent Deep Red Fluorescence Cytopainter (ab176736, abcam) for 20 minutes following the manufacturer's instructions and mixed to 1 million cells/mL in the different bioinks or DMEM/F12 media and murine ECM solution as controls. 70 µL cuvettes (BrandTech, 759220) were then filled with cell-laden bioinks, closed with parafilm and incubated at 37 °C, 5% CO2 for 1 or 6 h. Samples were rotated 90° immediately prior to imaging using confocal microscopy along the entire height of the cuvette chamber (5 mm). Images were stitched together and divided into four vertical sections of equal size. Cells in each section were counted using ImageJ/Fiji v1.52p (Wayne Rasband, NIH, USA) and the cell sedimentation coefficient calculated as previously published (n=3 technical replicates/condition).[118] Text taken from De Santis et al.[193]

Electron microscopy imaging

Scanning electron microscopy (SEM)

Alginate or rECM hydrogels (without cells) were lyophilized without further crosslinking to preferentially preserve alginate networks (LABCONCO freeze drier). Samples were sputter coated with gold (with 40 mA current for 120 s) (Cressington, Watford, U.K) before being mounted and examined in a Jeol JSM-7800F FEG-SEM. For experiments where cells were seeded on top of hydrogels, samples were fixed in glutaraldehyde while in the coated inserts, followed by graded series of ethanol dehydration and critical point drying. Samples were sputter-coated with gold-palladium (with 40 mA current for 120 s) (Cressington, Watford, U.K) before being mounted and examined in a Jeol JSM-7800F FEG-SEM (n=3/condition). Text taken from De Santis et al.[193]

Transmission electron microscopy

Alginate and rECM samples were fixed using 2% paraformaldehyde and 2% glutaraldehyde in 0.1 m Sorensen phosphate buffer for 24 hours and then washed in Sorensen buffer. Next samples were post-fixed in 1% osmium tetroxide, acetone dehydrated and finally, embedded in Polybed 812 epoxy resin. Ultrathin sections were cut using a Leica EM UC7 and mounted on Maxtaform H5 copper grids. The mounted sections were stained with 2% uranyl acetate and 1% lead citrate and imaged in a FEI Tecnai BioTwin 120 kV microscope.

FRESH printing

FRESH printing was performed as described previously[98] with modifications. Briefly, a Replicator 2X Experimental 3D Printer (845-9567, MakerBot) was modified by replacing the plastic filament extruder with a 3D-printed syringe-based extruder. Bioprinting of individual bioinks (i.e. single extrusion) was done using the earlier model of the syringe extruder (3DPX-002102, NIH 3D Print Exchange), whereas bioprinting of two cell types was done with an updated model (Replistruder v3.0, YouMagine.com). A 2.5 mL Hamilton GASTIGHT 1000 series Syringe (26209, Sigma) was mounted to the 3D-printed extruder equipped with a modified 27G needle (BD Microlance™). Pre-gel solutions were extruded into a 4°C cold 6% gelatin slurry containing 20 mM CaCl2 prepared as previously described5. All 3D models were designed using Blender v2.79 (www.blender.org). STL files were exported from blender and post-processed using KISSlicer (www.kisslicer.com/) to generate the G-code at 50 µm-thick layers. Replicator G (replicat.org) or Simplify3D (www.simplify3d.com/) software were used to communicate the G-code to printer.

For single extrusion experiments, cells were fluorescently labelled with Cell Proliferation Staining Reagent Deep Red Fluorescence Cytopainter (Abcam) following the manufacturer's instructions. The bioinks were prepared by mixing the stained cells with 2 wt% alginate, mouse-hybrid, or human-hybrid solutions at a concentration of 10^6 cells/mL. Single extrusion was performed at approximately 0.14 µl/second and thermal imaging was done to monitor the 3D bioprinting process using a FLIR thermal camera (FLIR A655sc 25°, FLIR). For dual extrusion experiments, HBECs and HLSMCs were labelled respectively with Cell Proliferation Staining Reagent Blue and Deep Red Fluorescence Cytopainter (abcam) as above. Each bioink was separately prepared by mixing the stained cells with 2 wt% alginate or human-hybrid solutions at a concentration of 10^6 cells/mL for HLSMCs and $3x10^6$ cells/mL for HBECs. 3D bioprinting of dual extrusion was done at a speed of 0.17 µl/second. Bioprinted 3D constructs remained in gelatin slurry, prepared as previously described5, to crosslink for 30 minutes. The gelatin slurry was then dissolved at 37 °C. The 3D bioprinted airways (single or dual

extrusion) were maintained in a 24 well, 0.4 µm pore size, transwell plates (Corning Costar). Constructs were lifted to ALI after 7 days and supplemented with ALI basal media (PneumaCult) for 28 days with media changes every other day. Airway cross-sections were imaged using confocal microscopy (n=3 patients/condition). Text taken from De Santis et al.[193]

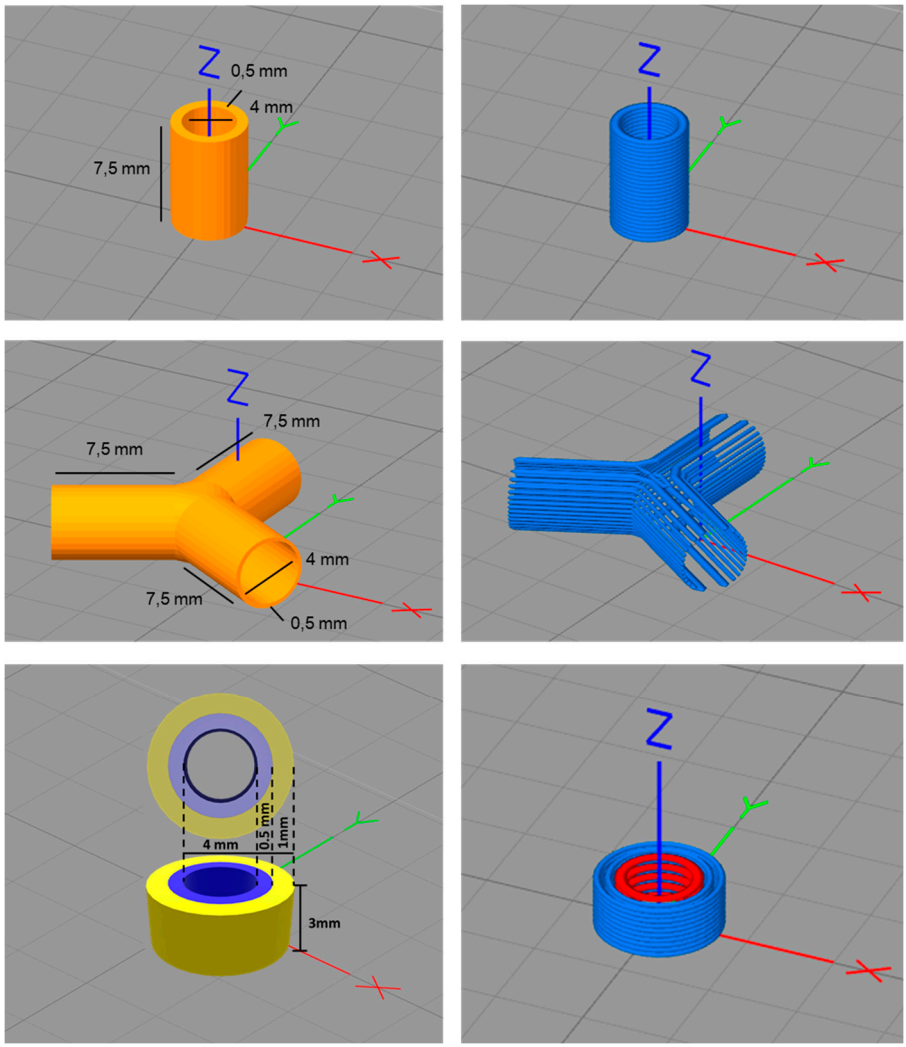

Figure 21 3D rendering of bioprinted constructs

(Left) Digital rendering of bioprinted single extrusion tube and branching structure and double extrusion tube. (Right) Trace of extrusion movement shown in blue for single extrusion and in red and blue for double extrusion. Figure and text taken from De Santis et al, 2020 with permission.[193]

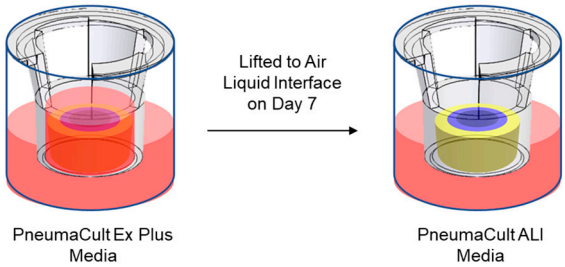

Figure 22 Bioprinted constructs lifted to Air Liquid Interface (ALI)

Dual extrusion bioprinted constructs are placed in inserts with PneumaCult Expansion Plus media supplemented both in the inner and outer chamber. After 7 days of culture the bioprinted constructs are lifted to ALI with PneumaCult ALI media supplemented only in the outer chamber. The bioprinted airways were kept in culture for 28 days with media changes every other day. Figure and text taken from De Santis et al, 2020 with permission.[193]

3D bioprinting simulations

Shear stress profiles during 3D printing were estimated by performing fluid dynamics simulations using the finite element method with COMSOL Multiphysics® 5.5 to model extrusion through the syringe. The system geometry was constructed as a 3.5 cm long needle (ID = 0.34 mm) and 3.5 cm of the syringe (ID = 7.35 mm) in polar coordinates (axisymmetric). To determine the velocity profiles, the Navier-Stokes equations were solved with a P2-P1 Lagrange elements (2nd order for velocity, 1st order for pressure). Simulations considered an inelastic response of the bioinks and used experimentally determined effective viscosity versus shear rate data as an input for rECM bioinks with a polynomial interpolation due to the complex rheological behaviour while for alginate a power-law expression was found to be suitable to describe the data. The mesh consisted of 200,000 quadrilateral elements after successive refinement.

$$\rho\vec{u}\cdot\nabla\vec{u} = -\nabla p + \nabla\cdot\mu(\dot{\gamma})[(\nabla\vec{u}) + (\nabla\vec{u})^{\mathrm{T}}]$$

where ρ is the fluid density (kg/m3), u ⃗ is the velocity vector (m s-1), p is the pressure (Pa), μ(γ ̇) is the shear rate dependent effective viscosity (Pa·s) and γ ̇ is the shear rate (1 s-1). The shear rate was estimated using the following equation:

$$\dot{\gamma} = \sqrt{2\mathbf{S}:\mathbf{S}} \text{ where } \mathbf{S} = \frac{1}{2}[(\nabla\vec{u}) + (\nabla\vec{u})^{\mathrm{T}}]$$

with a minimum value of 0.005 1 s-1 used for assessing viscosity, corresponding to the minimum value measured during rheological characterization of the inks.
The magnitude of the local average shear-stress was then determined by:

$$\tau = \mu(\dot{\gamma})\dot{\gamma}$$

Text taken from De Santis et al.[193]

Live Dead staining

Staining of live and dead bioprinted HBECs occurred directly after bioprinting into disk shapes (⌀: 6mm, h:2mm, print speed: 0.18 µL s-1), from bioinks containing 1 million cells mL-1. Calcein-AM (0.33 µM) (Sigma Aldrich) was used for live staining and propidium iodide (1 µg mL-1) (Sigma Aldrich) was used for dead staining. 3 images per sample (3 samples per condition) were obtained using confocal microscopy. The number of live/dead cells in each image was quantified using ImageJ/Fiji v1.52p (Wayne Rasband, NIH, USA)). Text modified from De Santis et al.[193]

Chick chorioallantoic membrane (CAM) assay

Fertilized eggs from Lohmann Brown chicken were commercially purchased and incubated in a BINDER incubator at 37.5 °C with constant humidity. A small window in the shell was opened on embryonic day 3 (E3) under aseptic conditions. The window was resealed with adhesive tape and eggs were returned to the incubator. On day E6, 10 µL of hydrogels (alginate, hybrid hydrogel and BME (Cultrex®)) or parafilm were placed on top of the CAM. Eggs were resealed and returned to the incubator. On day E8, Ringer's salt solution was added on top of the CAM to prevent dehydration. Pictures were taken with a brightfield microscope (LEICA S9i) on E6 and E10 and analysed with ImageJ/Fiji v1.52p (Wayne Rasband, NIH, USA)) by three independent investigators in a blinded fashion (n=7-11/ condition). Text taken from De Santis et al.[193]

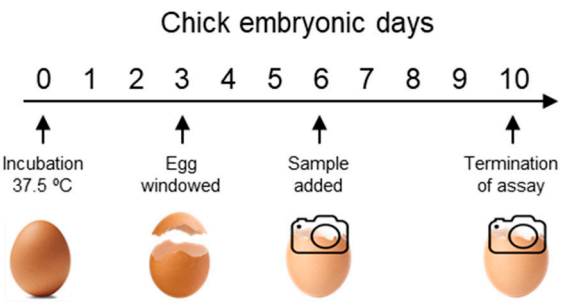

Figure 23 Chick chorioallantoic membrane (CAM) assay (taken from De Santis et al, 2020 with permission).[193]

Subcutaneous Implantations

Alginate and mouse rECM disks (⌀: 6mm, h:2mm, print speed: 0.18 µL s-1) were 3D printed as described above and subcutaneously implanted (6 disks/mouse) into FoxN1 KO BALB/C background nude mice (animal ethics approval number: M15485-18). Macrophage response on day 7 was assessed using flow cytometry (LSRII/FORTESA) for the following markers: CD45+, CD11b+, F4/80+, CD11c+/-, CD206+/- by pooling 3 constructs/condition from one mouse together and dissociating with EDTA (50 mM) (n=10 mice/condition). Cell concentrations were then measured using an automatic cell counter (Countess™ II FL Automated Cell Counter, Invitrogen) followed by 1-hour incubation with primary antibodies. M1 macrophages were defined by CD45+, CD11b+, F4/80+ and CD11c+. M2 macrophages were defined by CD45+, CD11b+, F4/80+, CD11c- and CD206+. M0 (non-polarized) macrophages were defined by CD45+, CD11b+, F4/80+ and CD11c-. Details of antibodies used can be found in Table 1. Implanted hydrogels on day 28 were explanted and fixed with 10% formalin for 4 hours (n=3 mice/condition). Text taken from De Santis et al.[193]

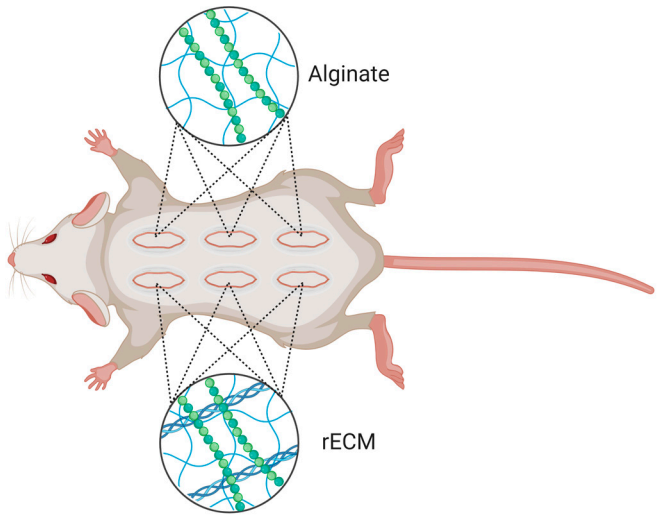

Figure 24 Subcutanous implantation of alginate and rECM hydrogels. Created with BioRender.com

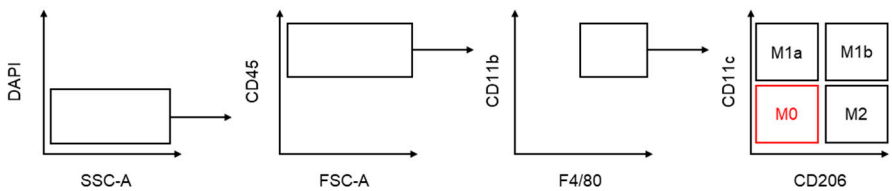

Figure 25 Flow cytometry gating strategy illustrating macrophage phenotyping (taken from De Santis et al, 2020 with permission).[193]

Table 3. Flow cytometry antibodies for subcutaneous implantations (taken from De Santis et al, 2020 with permission).[193]

Antibody	Cells	Dilution	Reference Biolegend
CD11b	Type I Macrophages, Monocytes, Dendritic cells, Granulocytes	1:75	101262
CD11c	Dendritic cells, Natural Killer cells	1:100	117318
CD206	Type II Macrophages	1:125	141712
CD45	Natural Killer cells, White Blood cells	1:200	147706
F4/80	Dendritic cells, Type I and II Macrophages	1:100	123110

Light-Sheet microscopy

Subcutaneously implanted hydrogels were processed using the iDISCO protocol as previously described.[212] Briefly, samples were washed with PBS and fixed at room temperature (RT) with 10% formalin for 1 hour. After extensive washing with PBS, the samples were dehydrated in a methanol/PBS series (20%, 40%, 60%, 80%, 100%, 100% for 1hr each), incubated in 66% dichloromethane / 33% Methanol for 3 hours, 100% dichloromethane for 30 minutes and in DiBenzyl Ether until before imaging. The samples were imaged submerged in dibenzyl ether using an Ultra Microscope II (LaVision Biotec) equipped with a 4x dipping objective (excitation/emission: 488/525 nm). 3D renditions and movies were created with Arivis Vision 4 D 3.1 (Arivis AG). Text taken from De Santis et al.[193]

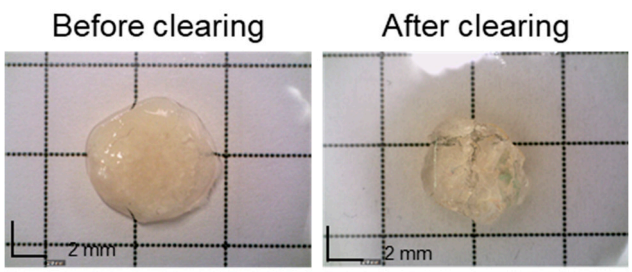

Figure 26 Optical clearing of alginate hydrogels

Human bronchial epithelial cells

HBECs isolation

Human bronchial epithelial cells (HBECs) were isolated from discarded surgical waste from the bronchial anastomosis of donor lungs (Lund Dnr 2017/396). The average age of the patients was 45, with two females and one male. Bronchi were dissected from the surrounding tissue and trimmed into smaller (1-2 cm2) pieces and immersed in PBS with the addition of 200 mg/L streptomycin, 200 U/mL penicillin, 5 µg/mL Amphotericin B and 100 µg/mL Gentamicin. Airway pieces were then incubated in 0.1% protease-DMEM/F12 media overnight at 4 °C and at 37 °C for 1 hour. Cells were isolated from the lumen by rinsing with DMEM/F12 media supplemented with 10% FBS and by rubbing gently on the walls with a pipette tip. The cell pellet was treated with DNase for 30 minutes at 37 °C, filtered through a 100 µm cell strainer and seeded in collagen I coated T75 flasks (~ 2 million cells/flask) for expansion with PneumaCult Expansion plus basal media supplemented with 0.1 µg/mL hydrocortisone, 100 mg/L streptomycin, 100 U/mL penicillin, 2.50 µg/mL Amphotericin B and 50 µg/mL Gentamicin. Expansion media was changed every other day. Text taken from De Santis et al.[193]

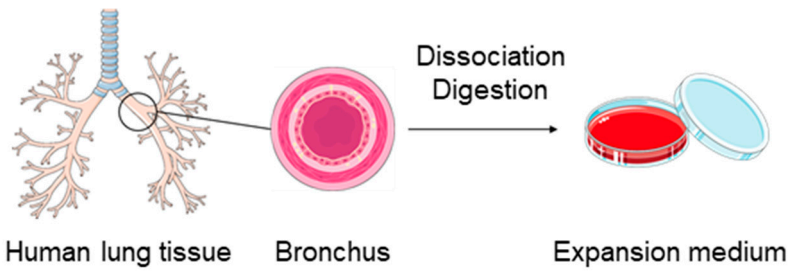

Figure 27 Human Bronchial Epithelial Cell (HBECs) isolation and expansion

HBECs were isolated from discarded surgical waste of healthy human bronchi using both mechanic and enzymatic digestion. The resulting cells were expanded with PneumaCult Expansion Plus media and then stored in liquid nitrogen at low passages (P1/P2). Figure and text taken from De Santis et al, 2020 with permission.[193]

HBECs ALI culture and seeding onto hydrogels

~ 80% confluent HBECs were lifted from the flasks and seeded onto alginate, hybrid or PureCol (consisting of collagen I and III coated) 24 well, 0.4 µm pore size, transwell plates (Corning Costar) at a 100'000 cells/ insert. Cells were expanded with the antibiotic and hydrocortisone supplemented PneumaCult Expansion plus basal media until a confluent pseudostratified layer was formed and then lifted to ALI culture using 0.2 µg/mL heparin, 0.5 µg/mL hydrocortisone and antibiotic (100 mg/L streptomycin, 100 U/mL penicillin, 2.50 µg/mL Amphotericin B and 50

µg/mL Gentamicin) supplemented PneumaCult ALI basal media up to 35 days. ALI media was changed every other day. Hydrogel coated inserts were fixed on day 28 with 10% formalin for 1 hour at RT (n=3 patients/condition). Text modified from De Santis et al.[193]

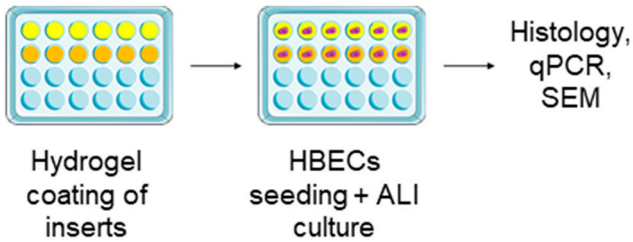

Figure 28 HBECs seeding on hydrogel coated inserts

Hydrogel coated inserts were seeded with HBECs at a 100'000 cell/insert concentration and expanded for 7 days with PneumaCult Expansion plus basal media. Once, a confluent pseudostratified layer was formed, the cells in the inserts were lifted to ALI.HBECs were kept in ALI culture for 35 days with media changes every other day and then processed for histology, RNA and electron microscopy analysis. Figure and text taken from De Santis et al, 2020 with permission.[193]

Real-time RT-qPCR

RNA was extracted from snap-frozen hydrogels using 50 mM EDTA homogenization, TRIzol and chloroform extraction, following with RNeasy Micro Kit (Qiagen). The RNA was reverse-transcribed to cDNA using iScript™ Reverse Transcription Supermix (BioRad), and then run in duplicate on a BioRad CFX96TM Real-Time system. For HBECs the relative expression of CC10, KRT5, KRT14, MUC5AC and MUC5B was calculated as $2^{-\Delta Ct}$, with ΔCt calculated by subtracting the average Ct of RPLP0 gene as a housekeeping control from the experimental sample Ct (n=3 patients/condition (P1, P2, P3). For subcutaneously implanted hydrogels the relative expression of Arginase, IL10 and CD31 was calculated as $2^{-\Delta Ct}$, with ΔCt calculated by subtracting the average Ct of HPRT gene as a housekeeping control from the experimental sample Ct (n=3-5/group). Text taken from De Santis et al.[193]

Histology

Alginate and hybrid samples were washed in PBS three times and OCT embedded in order to facilitate processing of 5 µm thin cryocuts, mounted on glass microscopic slides, for histological and immunofluorescence staining. H&E, Masson's Trichrome and Alizarin Red stainings were performed using standard methods[213,214]

and images were acquired on a Nikon H600L brightfield microscope. For immunofluorescence stainings, cryocuts were washed with PBS before being blocked for 1 hour with 5 wt% bovine serum albumin (Sigma) in PBS, and incubated with primary antibody overnight at 4 °C (Table 3) After incubation with an appropriate secondary antibody for 1 hour, images were acquired on a Nikon A1+ confocal system at Lund University Bioimaging center. Text modified from De Santis et al.[193]

Table 4. Primary antibodies for immunofluorescence

Antibody	Dilution	Reference	Company
Acetyl-α-tubulin	1:800	5335S	Cell Signaling
Arginase	1:50	ab60176	Abcam
CD3	1:100	ab5690	Abcam
CD4	1:100	ab203034	Abcam
CD68	1:50	ab31630	Abcam
iNOS	1:100	ab115819	Abcam
KRT5	1:400	ab52635	Abcam
Muc5ac	1:500	ab3649	Abcam
p63	1:300	ab124762	Abcam

Statistical analysis

Student t- tests were performed to compare the means of two normally distributed groups (alginate and rECM). Paired student t-test was performed to compare the means of alginate and rECM when the measurements were done using the same batch of alginate and the same cell passage number. One-way ANOVA was performed to test for statistical significance between the means of three or more normally distributed groups with a post hoc Tukey's multiple comparison test. Wilcoxon signed rank tests were used to assess significance between two non-normally distributed groups. In the case of graphs showing growth rates in percentages, we tested the difference in mean between the conditions. All graphs show the mean and ± standard deviation (SD). Statistics were performed and graphs generated using GraphPad Prism 7 (GraphPad Software). P-values ≤ 0.05 are represented with (*), p-values ≤ 0.01 with (**), p-values ≤ 0.001 with (***) and p-values ≤ 0.0001 with (****).Text taken from De Santis et al.[193]

Acknowledgements

Darcy Wagner, thank you. Moving to Sweden to your lab and joining this adventure has been incredible. Thank you for giving me the opportunity to grow and to work in such a nice environment. I learnt a lot during these 4 years, and this would not have been possible without your continuous support.

Thank you to **Gunilla** Westergren-Thorsson and **Sandra** Lindstedt my co-supervisors for your support throughout the PhD.

Sofie Mohlin, thank you for being the most amazing mentor. I am so grateful for all of your support and incredibly valuable advice about both academia and life.

Thank you to all of the LBR group and collaborators including **Manlio**, **Sujeeth** and **Paul**. A special thank you to my fellow PhD students, **Hani**, **Iran**, **Victoria** and **Niko** and to all the Postdocs in the LBR especially **John**, **Sinem**, **Deniz** and **Kristina**. I have learnt a lot from each of you and it has been a pleasure to work with you.

Thank you to **Ingela**, for being always ready to help with all types of matters. I truly appreciate it. Your kindness will always be remembered.

Thank you **Maggie**, for teaching me how to be a supervisor and for bringing all that positive energy to the lab.

Thank you to the C12 and B10 floor including **Anki** and **Kinga**, and the B10 girls **Sophie**, **Shayini**, **Sara**, **Ella** and **Andrea.**

Thank you to the MK lab with a special thank you to **Aina**, **Rita**, **Mareike**, **Chiharu** and **Melanie** Königshoff.

Thank you to LBIC, especially **Sebastian** Wasserstrom and **Lina** Gefors for their help in all imaging related things.

Thank you to **Stina** Oredsson for involving me in the biology teaching program and **Atena** and **John** for being my teaching partners. It was great fun to teach the labs and I learnt a lot.

Anna Niroomand, you funny funny girl. Thank you for dragging me out at night to do fun youthful things. **Franzi**, thank you for your support!

I would like to thank all the lovely people I have met in Lund University these past few years. A special thank you to “Comida de mi vida” aka PhD Support group for all the after work beers, pub quizzes, dinner parties and Swedish (and Icelandic and Maltese) adventures. This PhD would not have been the same without you.

Alex, for passing by for “quick chats” during B10 corridor walks, for your amazing (!) dinner parties and for being the loveliest person.

Ana, for bringing so much positivity to this group. For always being active and ready to do things.

Kat, for being there for me at all times. Your friendship means so much to me and rest assured I will be using your services as agony aunt for many years to come (hurray!).

Laura, for being a great friend, for being as competitive as me in board games (making for a great team), and for saving that RNA isolation disaster. Panel 3d in paper I is there thanks to you.

Maria, for being so caring and sweet. Your kindness is truly one of a kind and will always be remembered.

Marta, for introducing me to social life in Lund (and Malmö). The day I came to pick up those mice was my lucky day! For being my go to semi-Swedish person, for being so kind (and for taking care of those mice).

Matilde and **Martino**, my Italian co-representatives in a very Spanish group. Thank you for the fun dinner parties and hikes all around Skåne.

Mo, for our hot chocolate transitioned into tea breaks and talks about life, and assuring me that everything will be okay in the end.

Myriam, for making me laugh (sometimes too hard) and for being so caring. For teaching me about “bomba de humo”, a social skill I shall cherish.

Flavia, how lucky I am to have met you at the beginning of this PhD. Thank you for your support during our highs and our lows. For being only one Whatsapp voicenote or call away and for your indispensable advice. I am lucky to have you as friend.

Claudio, Thank you. For being there for me every day. For making long distance work. For never “clipping my wings” and for pushing me to achieve great things. For all of our English, German, Italian and Swedish adventures. I cannot wait to see what else life has in store for us.

Alla mia famiglia, **Mamma, papá** e **Laura** questa tesi é dedicata a voi. Grazie per avermi sostenuti in questi anni e per avere creduto in me. Vi voglio tanto bene.

References

1. *European Respiratory Society. The economic burden of lung disease. ERS White Book*, 2017).
2. Wang, H. *et al.* Global, regional, and national life expectancy, all-cause mortality, and cause-specific mortality for 249 causes of death, 1980–2015: a systematic analysis for the Global Burden of Disease Study 2015. *The Lancet* **388**, 1459-1544, (2016).
3. Torre, L. A. *et al.* Global cancer statistics, 2012. *CA: a cancer journal for clinicians* **65**, 87-108, (2015).
4. Pearce, N. *et al.* Worldwide trends in the prevalence of asthma symptoms: phase III of the International Study of Asthma and Allergies in Childhood (ISAAC). *Thorax* **62**, 758-766, (2007).
5. Burney, P. G. J., Patel, J., Newson, R., Minelli, C. & Naghavi, M. Global and regional trends in COPD mortality, 1990–2010. *European Respiratory Journal* **45**, 1239-1247, (2015).
6. Wagner, D. E. *et al.* Comparative decellularization and recellularization of normal versus emphysematous human lungs. *Biomaterials* **35**, 3281-3297, (2014).
7. Yusen, R. D. *et al.* The Registry of the International Society for Heart and Lung Transplantation: Thirty-second Official Adult Lung and Heart-Lung Transplantation Report 2015; Focus Theme: Early Graft Failure. *The Journal of heart and lung transplantation : the official publication of the International Society for Heart Transplantation* **34**, 1264-1277, (2015).
8. De Santis, M. M., Bölükbas, D. A., Lindstedt, S. & Wagner, Darcy E. How to build a lung: latest advances and emerging themes in lung bioengineering. *European Respiratory Journal* **52**, 1601355, (2018).
9. Franks, T. J. *et al.* Resident cellular components of the human lung: current knowledge and goals for research on cell phenotyping and function. *Proceedings of the American Thoracic Society* **5**, 763-766, (2008).
10. Adams, T. S. *et al.* Single-cell RNA-seq reveals ectopic and aberrant lung-resident cell populations in idiopathic pulmonary fibrosis. *Science advances* **6**, eaba1983, (2020).
11. Habermann, A. C. *et al.* Single-cell RNA sequencing reveals profibrotic roles of distinct epithelial and mesenchymal lineages in pulmonary fibrosis. *Science advances* **6**, eaba1972, (2020).
12. Reyfman, P. A. *et al.* Single-Cell Transcriptomic Analysis of Human Lung Provides Insights into the Pathobiology of Pulmonary Fibrosis. *American journal of respiratory and critical care medicine* **199**, 1517-1536, (2019).

13. Schamberger, A. C., Staab-Weijnitz, C. A., Mise-Racek, N. & Eickelberg, O. Cigarette smoke alters primary human bronchial epithelial cell differentiation at the air-liquid interface. *Sci Rep* **5**, 8163, (2015).
14. Brekman, A., Walters, M. S., Tilley, A. E. & Crystal, R. G. FOXJ1 Prevents Cilia Growth Inhibition by Cigarette Smoke in Human Airway Epithelium In Vitro. *American Journal of Respiratory Cell and Molecular Biology* **51**, 688-700, (2014).
15. Baarsma, H. A. *et al.* Noncanonical WNT-5A signaling impairs endogenous lung repair in COPD. *Journal of Experimental Medicine* **214**, 143-163, (2016).
16. Skronska-Wasek, W. *et al.* Reduced Frizzled Receptor 4 Expression Prevents WNT/β-Catenin–driven Alveolar Lung Repair in Chronic Obstructive Pulmonary Disease. *American journal of respiratory and critical care medicine* **196**, 172-185, (2017).
17. De Rose, V., Molloy, K., Gohy, S., Pilette, C. & Greene, C. M. Airway Epithelium Dysfunction in Cystic Fibrosis and COPD. *Mediators Inflamm* **2018**, 1309746-1309746, (2018).
18. Fahy, J. V. & Locksley, R. M. The Airway Epithelium As a Regulator of Th2 Responses in Asthma. *American journal of respiratory and critical care medicine* **184**, 390-392, (2011).
19. Boat, T. F. & Cheng, P. W. Epithelial cell dysfunction in cystic fibrosis: implications for airways disease. *Acta paediatrica Scandinavica. Supplement* **363**, 25-29; discussion 29-30, (1989).
20. Ota, C. *et al.* Dynamic expression of HOPX in alveolar epithelial cells reflects injury and repair during the progression of pulmonary fibrosis. *Scientific Reports* **8**, 12983, (2018).
21. Smirnova, N. F. *et al.* Detection and quantification of epithelial progenitor cell populations in human healthy and IPF lungs. *Respir Res* **17**, 83-83, (2016).
22. Hiemstra, P. S., Tetley, T. D. & Janes, S. M. Airway and alveolar epithelial cells in culture. *European Respiratory Journal*, 1900742, (2019).
23. Weibel, E. R. Lung morphometry: the link between structure and function. *Cell and Tissue Research* **367**, 413-426, (2017).
24. Weibel, E. R. (Academic Press, 1963).
25. Crystal, R. G., Randell, S. H., Engelhardt, J. F., Voynow, J. & Sunday, M. E. Airway epithelial cells: current concepts and challenges. *Proc Am Thorac Soc* **5**, 772-777, (2008).
26. Widdicombe, J. H. & Wine, J. J. Airway Gland Structure and Function. *Physiological Reviews* **95**, 1241-1319, (2015).
27. Donaldson, S. H., Corcoran, T. E., Laube, B. L. & Bennett, W. D. Mucociliary Clearance as an Outcome Measure for Cystic Fibrosis Clinical Research. *Proceedings of the American Thoracic Society* **4**, 399-405, (2007).
28. Montoro, D. T. *et al.* A revised airway epithelial hierarchy includes CFTR-expressing ionocytes. *Nature* **560**, 319-324, (2018).
29. Choksi, S. P., Lauter, G., Swoboda, P. & Roy, S. Switching on cilia: transcriptional networks regulating ciliogenesis. *Development* **141**, 1427-1441, (2014).
30. Satir, P. & Christensen, S. T. Overview of Structure and Function of Mammalian Cilia. *Annual Review of Physiology* **69**, 377-400, (2007).

31. Maruta, H., Greer, K. & Rosenbaum, J. L. The acetylation of alpha-tubulin and its relationship to the assembly and disassembly of microtubules. *Journal of Cell Biology* **103**, 571-579, (1986).
32. Piperno, G., LeDizet, M. & Chang, X. J. Microtubules containing acetylated alpha-tubulin in mammalian cells in culture. *Journal of Cell Biology* **104**, 289-302, (1987).
33. Audie, J. P. *et al.* Expression of human mucin genes in respiratory, digestive, and reproductive tracts ascertained by in situ hybridization. *The journal of histochemistry and cytochemistry : official journal of the Histochemistry Society* **41**, 1479-1485, (1993).
34. Rock, J. R., Randell, S. H. & Hogan, B. L. M. Airway basal stem cells: a perspective on their roles in epithelial homeostasis and remodeling. *Disease Models & Mechanisms* **3**, 545-556, (2010).
35. Singh, G. & Katyal, S. L. An immunologic study of the secretory products of rat Clara cells. *The journal of histochemistry and cytochemistry : official journal of the Histochemistry Society* **32**, 49-54, (1984).
36. Patton, S. E., Gilmore, L. B., Jetten, A. M., Nettesheim, P. & Hook, G. E. R. Biosynthesis and Release of Proteins by Isolated Pulmonary Clara Cells. *Experimental Lung Research* **11**, 277-294, (1986).
37. Williams, M. C. Alveolar Type I Cells: Molecular Phenotype and Development. *Annual Review of Physiology* **65**, 669-695, (2003).
38. Rubins, J. B. Alveolar Macrophages. *American journal of respiratory and critical care medicine* **167**, 103-104, (2003).
39. Liebler, J. M. *et al.* Combinations of differentiation markers distinguish subpopulations of alveolar epithelial cells in adult lung. *American journal of physiology. Lung cellular and molecular physiology* **310**, L114-120, (2016).
40. Possmayer, F. A Proposed Nomenclature for Pulmonary Surfactant-associated Proteins. *American Review of Respiratory Disease* **138**, 990-998, (1988).
41. Chin, L. Y. M. *et al.* Human airway smooth muscle is structurally and mechanically similar to that of other species. *European Respiratory Journal* **36**, 170-177, (2010).
42. Gunst, S. J. & Panettieri, R. A., Jr. Point: alterations in airway smooth muscle phenotype do/do not cause airway hyperresponsiveness in asthma. *J Appl Physiol (1985)* **113**, 837-839, (2012).
43. Paré, P. D. & Mitzner, W. Counterpoint: alterations in airway smooth muscle phenotype do not cause airway hyperresponsiveness in asthma. *J Appl Physiol (1985)* **113**, 839-842, (2012).
44. Gu, Q. & Lee, L. Y. in *Encyclopedia of Respiratory Medicine* (Academic Press, 2006).
45. Doeing, D. C. & Solway, J. Airway smooth muscle in the pathophysiology and treatment of asthma. *J Appl Physiol (1985)* **114**, 834-843, (2013).
46. Langer, R. & Vacanti, J. P. Tissue engineering. *Science (New York, N.Y.)* **260**, 920-926, (1993).
47. Atala, A., Bauer, S. B., Soker, S., Yoo, J. J. & Retik, A. B. Tissue-engineered autologous bladders for patients needing cystoplasty. *Lancet (London, England)* **367**, 1241-1246, (2006).

48. Shin'oka, T. *et al.* Midterm clinical result of tissue-engineered vascular autografts seeded with autologous bone marrow cells. *The Journal of thoracic and cardiovascular surgery* **129**, 1330-1338, (2005).
49. Firth, A. L. *et al.* Generation of multiciliated cells in functional airway epithelia from human induced pluripotent stem cells. *Proceedings of the National Academy of Sciences* **111**, E1723-E1730, (2014).
50. Wong, A. P. *et al.* Directed differentiation of human pluripotent stem cells into mature airway epithelia expressing functional CFTR protein. *Nat Biotechnol* **30**, 876-882, (2012).
51. Abo, K. M. *et al.* Human iPSC-derived alveolar and airway epithelial cells can be cultured at air-liquid interface and express SARS-CoV-2 host factors. *bioRxiv*, 2020.2006.2003.132639, (2020).
52. Jacob, A. *et al.* Differentiation of Human Pluripotent Stem Cells into Functional Lung Alveolar Epithelial Cells. *Cell Stem Cell* **21**, 472-488.e410, (2017).
53. Huang, S. X. *et al.* Efficient generation of lung and airway epithelial cells from human pluripotent stem cells. *Nat Biotechnol* **32**, 84-91, (2014).
54. Gotoh, S. *et al.* Generation of alveolar epithelial spheroids via isolated progenitor cells from human pluripotent stem cells. *Stem cell reports* **3**, 394-403, (2014).
55. Dye, B. R. *et al.* In vitro generation of human pluripotent stem cell derived lung organoids. *eLife* **4**, (2015).
56. Hawkins, F. *et al.* Prospective isolation of NKX2-1-expressing human lung progenitors derived from pluripotent stem cells. *The Journal of clinical investigation* **127**, 2277-2294, (2017).
57. Takahashi, K. & Yamanaka, S. Induction of pluripotent stem cells from mouse embryonic and adult fibroblast cultures by defined factors. *Cell* **126**, 663-676, (2006).
58. Thomson, J. A. *et al.* Embryonic Stem Cell Lines Derived from Human Blastocysts. *Science (New York, N.Y.)* **282**, 1145-1147, (1998).
59. Jiang, D. *et al.* Two succeeding fibroblastic lineages drive dermal development and the transition from regeneration to scarring. *Nature Cell Biology* **20**, 422-431, (2018).
60. Burgstaller, G., Oehrle, B., Gerckens, M. & White, E. S. The instructive extracellular matrix of the lung: basic composition and alterations in chronic lung disease. *European Respiratory Journal* **50**, (2017).
61. Brown, B. N. & Badylak, S. F. Extracellular matrix as an inductive scaffold for functional tissue reconstruction. *Translational research: the journal of laboratory and clinical medicine* **163**, 268-285, (2014).
62. Crapo, P. M., Gilbert, T. W. & Badylak, S. F. An overview of tissue and whole organ decellularization processes. *Biomaterials* **32**, 3233-3243, (2011).
63. Fischer, S. N. *et al.* Organ-derived coatings on electrospun nanofibers as ex vivo microenvironments. *Biomaterials* **32**, 538-546, (2011).
64. Sorokin, L. The impact of the extracellular matrix on inflammation. *Nature reviews. Immunology* **10**, 712-723, (2010).

65. Suki, B., Ito, S., Stamenović, D., Lutchen, K. R. & Ingenito, E. P. Biomechanics of the lung parenchyma: critical roles of collagen and mechanical forces. *Journal of Applied Physiology* **98**, 1892-1899, (2005).
66. De Santis, M. M. & Wagner, D. E. Collagen IV: a critical new starting point for engineering upper airways. *European Respiratory Journal* **55**, 2001130, (2020).
67. Suki, B. & Bates, J. H. Extracellular matrix mechanics in lung parenchymal diseases. *Respiratory physiology & neurobiology* **163**, 33-43, (2008).
68. Faffe, D. S. & Zin, W. A. Lung Parenchymal Mechanics in Health and Disease. *Physiological Reviews* **89**, 759-775, (2009).
69. Wagenseil, J. E. & Mecham, R. P. New insights into elastic fiber assembly. *Birth Defects Research Part C: Embryo Today: Reviews* **81**, 229-240, (2007).
70. Annoni, R. *et al.* Extracellular matrix composition in COPD. *European Respiratory Journal* **40**, 1362-1373, (2012).
71. Roche, W. R., Beasley, R., Williams, J. H. & Holgate, S. T. Subepithelial fibrosis in the bronchi of asthmatics. *Lancet (London, England)* **1**, 520-524, (1989).
72. Mauad, T. *et al.* Abnormal alveolar attachments with decreased elastic fiber content in distal lung in fatal asthma. *American journal of respiratory and critical care medicine* **170**, 857-862, (2004).
73. Gilbert, T. W., Sellaro, T. L. & Badylak, S. F. Decellularization of tissues and organs. *Biomaterials* **27**, 3675-3683, (2006).
74. Wagner, D. E. *et al.* Can stem cells be used to generate new lungs? Ex vivo lung bioengineering with decellularized whole lung scaffolds. *Respirology (Carlton, Vic.)* **18**, 895-911, (2013).
75. Petersen, T. H. *et al.* Tissue-engineered lungs for in vivo implantation. *Science (New York, N.Y.)* **329**, 538-541, (2010).
76. Booth, A. J. *et al.* Acellular normal and fibrotic human lung matrices as a culture system for in vitro investigation. *American journal of respiratory and critical care medicine* **186**, 866-876, (2012).
77. O'Neill, J. D. *et al.* Decellularization of human and porcine lung tissues for pulmonary tissue engineering. *The Annals of thoracic surgery* **96**, 1046-1055; discussion 1055-1046, (2013).
78. Nichols, J. E. *et al.* Production and assessment of decellularized pig and human lung scaffolds. *Tissue engineering. Part A* **19**, 2045-2062, (2013).
79. Price, A. P. *et al.* Automated decellularization of intact, human-sized lungs for tissue engineering. *Tissue engineering. Part C, Methods* **21**, 94-103, (2015).
80. Parker, M. W. *et al.* Fibrotic extracellular matrix activates a profibrotic positive feedback loop. *The Journal of clinical investigation* **124**, 1622-1635, (2014).
81. Wagner, D. E. *et al.* Three-dimensional scaffolds of acellular human and porcine lungs for high throughput studies of lung disease and regeneration. *Biomaterials* **35**, 2664-2679, (2014).
82. Gilpin, S. E. *et al.* Perfusion decellularization of human and porcine lungs: bringing the matrix to clinical scale. *The Journal of heart and lung transplantation : the official publication of the International Society for Heart Transplantation* **33**, 298-308, (2014).

83. Gilpin, S. E. *et al.* Enhanced lung epithelial specification of human induced pluripotent stem cells on decellularized lung matrix. *The Annals of thoracic surgery* **98**, 1721-1729; discussion 1729, (2014).
84. Balestrini, J. L. *et al.* Comparative biology of decellularized lung matrix: Implications of species mismatch in regenerative medicine. *Biomaterials* **102**, 220-230, (2016).
85. Wallis, J. M. *et al.* Comparative assessment of detergent-based protocols for mouse lung de-cellularization and re-cellularization. *Tissue engineering. Part C, Methods* **18**, 420-432, (2012).
86. Petersen, T. H., Calle, E. A., Colehour, M. B. & Niklason, L. E. Matrix composition and mechanics of decellularized lung scaffolds. *Cells, tissues, organs* **195**, 222-231, (2012).
87. Zvarova, B. *et al.* Residual Detergent Detection Method for Nondestructive Cytocompatibility Evaluation of Decellularized Whole Lung Scaffolds. *Tissue engineering. Part C, Methods* **22**, 418-428, (2016).
88. Kawecki, M. *et al.* A review of decellurization methods caused by an urgent need for quality control of cell-free extracellular matrix' scaffolds and their role in regenerative medicine. *Journal of Biomedical Materials Research Part B: Applied Biomaterials*, n/a-n/a, (2017).
89. Badylak, S. F., Taylor, D. & Uygun, K. Whole-organ tissue engineering: decellularization and recellularization of three-dimensional matrix scaffolds. *Annual review of biomedical engineering* **13**, 27-53, (2011).
90. Freytes, D. O., Martin, J., Velankar, S. S., Lee, A. S. & Badylak, S. F. Preparation and rheological characterization of a gel form of the porcine urinary bladder matrix. *Biomaterials* **29**, 1630-1637, (2008).
91. Bonvillain, R. W. *et al.* A Nonhuman Primate Model of Lung Regeneration: Detergent-Mediated Decellularization and Initial In Vitro Recellularization with Mesenchymal Stem Cells. *Tissue Engineering Part A* **18**, 2437-2452, (2012).
92. Zhou, H. *et al.* Bioengineering Human Lung Grafts on Porcine Matrix. *Annals of surgery*, (2017).
93. Platz, J. *et al.* Comparative Decellularization and Recellularization of Wild-Type and Alpha 1,3 Galactosyltransferase Knockout Pig Lungs: A Model for Ex Vivo Xenogeneic Lung Bioengineering and Transplantation. *Tissue Engineering Part C Methods* **22**, 725-739, (2016).
94. Niu, D. *et al.* Inactivation of porcine endogenous retrovirus in pigs using CRISPR-Cas9. *Science (New York, N.Y.)*, (2017).
95. Nematollahi, Z. *et al.* Fabrication of Chitosan Silk-based Tracheal Scaffold Using Freeze-Casting Method. *Iranian biomedical journal*, (2017).
96. Lee, V. K. *et al.* Creating perfused functional vascular channels using 3D bio-printing technology. *Biomaterials* **35**, 8092-8102, (2014).
97. Bhattacharjee, T. *et al.* Writing in the granular gel medium. *Science advances* **1**, e1500655, (2015).
98. Hinton, T. J. *et al.* Three-dimensional printing of complex biological structures by freeform reversible embedding of suspended hydrogels. *Science advances* **1**, e1500758, (2015).

99. Feinberg, A. W. & Miller, J. S. Progress in three-dimensional bioprinting. *MRS Bulletin* **42**, 557-562, (2017).
100. Zhu, W. *et al.* Direct 3D bioprinting of prevascularized tissue constructs with complex microarchitecture. *Biomaterials* **124**, 106-115, (2017).
101. Kolesky, D. B., Homan, K. A., Skylar-Scott, M. A. & Lewis, J. A. Three-dimensional bioprinting of thick vascularized tissues. *Proceedings of the National Academy of Sciences of the United States of America* **113**, 3179-3184, (2016).
102. Hansen, C. J. *et al.* High-throughput printing via microvascular multinozzle arrays. *Advanced materials (Deerfield Beach, Fla.)* **25**, 96-102, (2013).
103. Pratt, A. B., Weber, F. E., Schmoekel, H. G., Muller, R. & Hubbell, J. A. Synthetic extracellular matrices for in situ tissue engineering. *Biotechnology and bioengineering* **86**, 27-36, (2004).
104. Hull, C. US 4575330 A. *Apparatus for production of three-dimensional objects by stereolithography* **11**, (1986).
105. Crump, S. S. (Google Patents, 1992).
106. Chimene, D., Kaunas, R. & Gaharwar, A. K. Hydrogel Bioink Reinforcement for Additive Manufacturing: A Focused Review of Emerging Strategies. *Advanced materials (Deerfield Beach, Fla.)* **32**, 1902026, (2020).
107. Morrison, R. J. *et al.* Mitigation of tracheobronchomalacia with 3D-printed personalized medical devices in pediatric patients. *Science Translational Medicine* **7**, 285ra264-285ra264, (2015).
108. Zopf, D. A., Hollister, S. J., Nelson, M. E., Ohye, R. G. & Green, G. E. Bioresorbable airway splint created with a three-dimensional printer. *The New England journal of medicine* **368**, 2043-2045, (2013).
109. Groll, J. *et al.* Biofabrication: reappraising the definition of an evolving field. *Biofabrication* **8**, 013001, (2016).
110. Groll, J. *et al.* A definition of bioinks and their distinction from biomaterial inks. *Biofabrication* **11**, 013001, (2018).
111. Taniguchi, D. *et al.* Scaffold-free trachea regeneration by tissue engineering with bio-3D printing. *Interactive cardiovascular and thoracic surgery*, (2018).
112. Cui, X., Breitenkamp, K., Finn, M. G., Lotz, M. & D'Lima, D. D. Direct human cartilage repair using three-dimensional bioprinting technology. *Tissue Engineering Part A* **18**, 1304-1312, (2012).
113. Cubo, N., Garcia, M., Del Canizo, J. F., Velasco, D. & Jorcano, J. L. 3D bioprinting of functional human skin: production and in vivo analysis. *Biofabrication* **9**, 015006, (2016).
114. Duan, B., Hockaday, L. A., Kang, K. H. & Butcher, J. T. 3D bioprinting of heterogeneous aortic valve conduits with alginate/gelatin hydrogels. *Journal of biomedical materials research. Part A* **101**, 1255-1264, (2013).
115. Norotte, C., Marga, F. S., Niklason, L. E. & Forgacs, G. Scaffold-free vascular tissue engineering using bioprinting. *Biomaterials* **30**, 5910-5917, (2009).
116. Weibel E. R. Lung cell biology. In: AP Fishman, ed. Handbook of Physiology. Section 3: The Respiratory System. Bethesda, *American Physiological Society*, 2011; pp. 47–91.

117. Hsia C. C., Hyde D. M., Weibel E. R. Lung structure and the intrinsic challenges of gas exchange. *Comprehensive Physiology* 2016; 6: 827–895.
118. Dubbin, K., Tabet, A. & Heilshorn, S. C. Quantitative criteria to benchmark new and existing bio-inks for cell compatibility. *Biofabrication* **9**, 044102-044102, (2017).
119. Highley, C. B., Rodell, C. B. & Burdick, J. A. Direct 3D Printing of Shear-Thinning Hydrogels into Self-Healing Hydrogels. *Adv Mater* **27**, 5075-5079, (2015).
120. Bhattacharjee, T. *et al.* Liquid-like Solids Support Cells in 3D. *ACS Biomaterials Science & Engineering* **2**, 1787-1795, (2016).
121. Afghah, F., Altunbek, M., Dikyol, C. & Koc, B. Preparation and characterization of nanoclay-hydrogel composite support-bath for bioprinting of complex structures. *Scientific Reports* **10**, 5257, (2020).
122. Jiang, T., Munguia-Lopez, J. G., Flores-Torres, S., Kort-Mascort, J. & Kinsella, J. M. Extrusion bioprinting of soft materials: An emerging technique for biological model fabrication. *Applied Physics Reviews* **6**, 011310, (2019).
123. McCormack, A., Highley, C. B., Leslie, N. R. & Melchels, F. P. W. 3D Printing in Suspension Baths: Keeping the Promises of Bioprinting Afloat. *Trends in Biotechnology* **38**, 584-593, (2020).
124. Moxon, S. R. *et al.* Suspended manufacture of biological structures. *Advanced materials (Deerfield Beach, Fla.)* **29**, 1605594, (2017).
125. O'Bryan, C. S. *et al.* Self-assembled micro-organogels for 3D printing silicone structures. *Sci Adv* **3**, e1602800, (2017).
126. Chimene, D., Lennox, K. K., Kaunas, R. R. & Gaharwar, A. K. Advanced Bioinks for 3D Printing: A Materials Science Perspective. *Annals of biomedical engineering* **44**, 2090-2102, (2016).
127. Malda, J. *et al.* 25th Anniversary Article: Engineering Hydrogels for Biofabrication. *Advanced materials (Deerfield Beach, Fla.)* **25**, 5011-5028, (2013).
128. Annabi, N. *et al.* 25th anniversary article: Rational design and applications of hydrogels in regenerative medicine. *Adv Mater* **26**, 85-123, (2014).
129. Lee, S. *et al.* Human-Recombinant-Elastin-Based Bioinks for 3D Bioprinting of Vascularized Soft Tissues. *Advanced materials (Deerfield Beach, Fla.)* **n/a**, 2003915.
130. Hinton, T. J. *et al.* Three-dimensional printing of complex biological structures by freeform reversible embedding of suspended hydrogels. *Science Advances* **1**, (2015).
131. Aderibigbe, B. A. & Buyana, B. Alginate in Wound Dressings. *Pharmaceutics* **10**, 42, (2018).
132. Wagner, D. E. *et al.* Design and Synthesis of an Artificial Pulmonary Pleura for High Throughput Studies in Acellular Human Lungs. *Cellular and molecular bioengineering* **7**, 184-195, (2014).
133. Rezende, R. A., Bártolo, P. J., Mendes, A. & Filho, R. M. Rheological behavior of alginate solutions for biomanufacturing. *Journal of Applied Polymer Science* **113**, 3866-3871, (2009).
134. Wu, Z. *et al.* Bioprinting three-dimensional cell-laden tissue constructs with controllable degradation. *Scientific Reports* **6**, 24474, (2016).

135. Montalbano, G. *et al.* Synthesis of bioinspired collagen/alginate/fibrin based hydrogels for soft tissue engineering. *Materials Science and Engineering: C* **91**, 236-246, (2018).
136. Capeling, M. M. *et al.* Nonadhesive Alginate Hydrogels Support Growth of Pluripotent Stem Cell-Derived Intestinal Organoids. *Stem cell reports* **12**, 381-394, (2019).
137. Kim, K. & Kim, M. S. An injectable hydrogel derived from small intestine submucosa as a stem cell carrier. *Journal of Biomedical Materials Research Part B: Applied Biomaterials* **104**, 1544-1550, (2016).
138. Pouliot, R. A. *et al.* Development and characterization of a naturally derived lung extracellular matrix hydrogel. *Journal of biomedical materials research. Part A* **104**, 1922-1935, (2016).
139. Wolf, M. T. *et al.* A hydrogel derived from decellularized dermal extracellular matrix. *Biomaterials* **33**, 7028-7038, (2012).
140. Medberry, C. J. *et al.* Hydrogels derived from central nervous system extracellular matrix. *Biomaterials* **34**, 1033-1040, (2013).
141. Cushing, M. C. & Anseth, K. S. Hydrogel Cell Cultures. *Science (New York, N.Y.)* **316**, 1133-1134, (2007).
142. Rothrauff, B. B. *et al.* Efficacy of thermoresponsive, photocrosslinkable hydrogels derived from decellularized tendon and cartilage extracellular matrix for cartilage tissue engineering. *J Tissue Eng Regen Med* **12**, e159-e170, (2018).
143. Mazzocchi, A., Devarasetty, M., Huntwork, R., Soker, S. & Skardal, A. Optimization of collagen type I-hyaluronan hybrid bioink for 3D bioprinted liver microenvironments. *Biofabrication* **11**, 015003, (2018).
144. Athirasala, A. *et al.* A dentin-derived hydrogel bioink for 3D bioprinting of cell laden scaffolds for regenerative dentistry. *Biofabrication* **10**, 024101, (2018).
145. Shin, J. H. & Kang, H.-W. The Development of Gelatin-Based Bio-Ink for Use in 3D Hybrid Bioprinting. *International Journal of Precision Engineering and Manufacturing* **19**, 767-771, (2018).
146. Lee, H. *et al.* Development of Liver Decellularized Extracellular Matrix Bioink for Three-Dimensional Cell Printing-Based Liver Tissue Engineering. *Biomacromolecules* **18**, 1229-1237, (2017).
147. Stichler, S. *et al.* Double printing of hyaluronic acid/poly(glycidol) hybrid hydrogels with poly(epsilon-caprolactone) for MSC chondrogenesis. *Biofabrication* **9**, 044108, (2017).
148. Gelinsky, M. in *3D Bioprinting for Reconstructive Surgery* (Woodhead Publishing, 2018).
149. Murphy, S. V., De Coppi, P. & Atala, A. Opportunities and challenges of translational 3D bioprinting. *Nature Biomedical Engineering*, (2019).
150. Polak, D. J. The use of stem cells to repair the injured lung. *British medical bulletin* **99**, 189-197, (2011).
151. Schwab, A. *et al.* Printability and Shape Fidelity of Bioinks in 3D Bioprinting. *Chemical Reviews* **120**, 11028-11055, (2020).
152. Suzanne, M. & Steller, H. Shaping organisms with apoptosis. *Cell death and differentiation* **20**, 669-675, (2013).

153. Tsuchiya, T. *et al.* Influence of pH on extracellular matrix preservation during lung decellularization. *Tissue Eng. Part C Methods* **20**, 1028-1036, (2014).
154. Brown, B. N. & Badylak, S. F. in *Regenerative Medicine Applications in Organ Transplantation* Ch. Chapter 11 - Biocompatibility and Immune Response to Biomaterials, (Academic Press, 2014).
155. Brown, B. N. & Badylak, S. F. Extracellular matrix as an inductive scaffold for functional tissue reconstruction. *Transl Res* **163**, 268-285, (2014).
156. Brown, B. N. *et al.* Macrophage phenotype as a predictor of constructive remodeling following the implantation of biologically derived surgical mesh materials. *Acta Biomater.* **8**, 978-987, (2012).
157. Brown, B. N., Ratner, B. D., Goodman, S. B., Amar, S. & Badylak, S. F. Macrophage polarization: an opportunity for improved outcomes in biomaterials and regenerative medicine. *Biomaterials* **33**, 3792-3802, (2012).
158. Brown, B. N., Valentin, J. E., Stewart-Akers, A. M., McCabe, G. P. & Badylak, S. F. Macrophage phenotype and remodeling outcomes in response to biologic scaffolds with and without a cellular component. *Biomaterials* **30**, 1482-1491, (2009).
159. Anderson, J. M. & Jones, J. A. Phenotypic dichotomies in the foreign body reaction. *Biomaterials* **28**, 5114-5120, (2007).
160. Anderson, J. M., Rodriguez, A. & Chang, D. T. Foreign body reaction to biomaterials. *Semin. Immunol.* **20**, 86-100, (2008).
161. Allman, A. J. *et al.* Xenogeneic extracellular matrix grafts elicit a TH2-restricted immune response. *Transplantation* **71**, 1631-1640, (2001).
162. Allman, A. J., McPherson, T. B., Merrill, L. C., Badylak, S. F. & Metzger, D. W. The Th2-restricted immune response to xenogeneic small intestinal submucosa does not influence systemic protective immunity to viral and bacterial pathogens. *Tissue engineering* **8**, 53-62, (2002).
163. Walsh, P. T., Strom, T. B. & Turka, L. A. Routes to transplant tolerance versus rejection; the role of cytokines. *Immunity* **20**, 121-131, (2004).
164. Illigens, B. M. *et al.* Dual effects of the alloresponse by Th1 and Th2 cells on acute and chronic rejection of allotransplants. *Eur J Immunol* **39**, 3000-3009, (2009).
165. Chung, L., Maestas, D. R., Housseau, F. & Elisseeff, J. H. Key players in the immune response to biomaterial scaffolds for regenerative medicine. *Advanced Drug Delivery Reviews* **114**, 184-192, (2017).
166. Mandavilli, S., Singh, B. B. & Sahmoun, A. E. Serum calcium levels, TRPM7, TRPC1, microcalcifications, and breast cancer using breast imaging reporting and data system scores. *Breast Cancer (Dove Med Press)* **2013**, 1-7, (2012).
167. Schoen, F. J. & Levy, R. J. Calcification of tissue heart valve substitutes: progress toward understanding and prevention. *The Annals of thoracic surgery* **79**, 1072-1080, (2005).
168. Singh, C. & Wang, X. Metal Ion-Loaded Nanofibre Matrices for Calcification Inhibition in Polyurethane Implants. *J Funct Biomater* **8**, 22, (2017).

169. Vasudev, S. C., Chandy, T., Mohanty, M., R., U. P. & Sharma, C. P. Inhibition of Bioprosthesis Calcification Due to Synergistic Effect of Fe/Mg Ions to Polyethylene Glycol Grafted Bovine Pericardium. *Journal of Biomaterials Applications* **16**, 93-107, (2001).
170. Singer, A. J. & Clark, R. A. F. Cutaneous Wound Healing. *New England Journal of Medicine* **341**, 738-746, (1999).
171. Gurtner, G. C., Werner, S., Barrandon, Y. & Longaker, M. T. Wound repair and regeneration. *Nature* **453**, 314-321, (2008).
172. Yokoyama, M. & Rafii, S. Setting up the dermis for scar-free healing. *Nature Cell Biology* **20**, 365-366, (2018).
173. Gonzales, K. A. U. & Fuchs, E. Skin and Its Regenerative Powers: An Alliance between Stem Cells and Their Niche. *Developmental Cell* **43**, 387-401, (2017).
174. Chang, W. G. & Niklason, L. E. A short discourse on vascular tissue engineering. *NPJ Regen. Med.* **2**, 7, (2017).
175. Pober, J. S. & Tellides, G. Participation of blood vessel cells in human adaptive immune responses. *Trends in immunology* **33**, 49-57, (2012).
176. Kant, C. D. *et al.* Both Rejection and Tolerance of Allografts Can Occur in the Absence of Secondary Lymphoid Tissues. *J. Immunol.* **194**, 1364-1371, (2015).
177. Delaere, P., Vranckx, J., Verleden, G., De Leyn, P. & Van Raemdonck, D. Tracheal allotransplantation after withdrawal of immunosuppressive therapy. *N. Engl. J. Med.* **362**, 138-145, (2010).
178. Butler, C. R. *et al.* Rapid Expansion of Human Epithelial Stem Cells Suitable for Airway Tissue Engineering. *Am. J. Respir. Crit. Care Med.* **194**, 156-168, (2016).
179. Delaere, P. R. *et al.* Learning curve in tracheal allotransplantation. *Am. J. Transplant* **12**, 2538-2545, (2012).
180. Chang, W. G. & Niklason, L. E. A short discourse on vascular tissue engineering. *npj Regenerative Medicine* **2**, 7, (2017).
181. Hamilton, N. J. I. *et al.* Bioengineered airway epithelial grafts with mucociliary function based on collagen IV- and laminin-containing extracellular matrix scaffolds. *Eur. Resp. J.*, 1901200, (2020).
182. De Santis, M. M. & Wagner, D. E. Collagen IV: a critical new starting point for engineering upper airways. *Eur. Resp. J.* **55**, 2001130, (2020).
183. Kilic, O. *et al.* A microphysiological model of the bronchial airways reveals the interplay of mechanical and biochemical signals in bronchospasm. *Nat. Biomed.* **3**, 532-544, (2019).
184. Chakir, J. *et al.* Bronchial mucosa produced by tissue engineering: a new tool to study cellular interactions in asthma. *J. Allergy. Clin. Immunol.* **107**, 36-40, (2001).
185. Crowley, C. *et al.* Surface modification of a POSS-nanocomposite material to enhance cellular integration of a synthetic bioscaffold. *Biomaterials* **83**, 283-293, (2016).
186. Pouliot, R. A. *et al.* Development and characterization of a naturally derived lung extracellular matrix hydrogel. *J. Biomed. Mater. Res. A* **104**, 1922-1935, (2016).
187. Hilster, R. H. J. d. *et al.* Human lung extracellular matrix hydrogels resemble the stiffness and viscoelasticity of native lung tissue. *Am. J. Physiol. Lung Cell Mol.* **318**, L698-L704, (2020).

188. Pati, F. *et al.* Printing three-dimensional tissue analogues with decellularized extracellular matrix bioink. *Nat. Commun.* **5**, 3935, (2014).
189. Hinton, T. J. *et al.* Three-dimensional printing of complex biological structures by freeform reversible embedding of suspended hydrogels. *Sci. Adv.* **1**, (2015).
190. Wagner, D. E. *et al.* Design and Synthesis of an Artificial Pulmonary Pleura for High Throughput Studies in Acellular Human Lungs. *Cell Mol. Bioeng.* **7**, 184-195, (2014).
191. Rezende, R. A., Bártolo, P. J., Mendes, A. & Filho, R. M. Rheological behavior of alginate solutions for biomanufacturing. *J. Appl. Polym.* **113**, 3866-3871, (2009).
192. Utracki, L. A. *Polymer Blends Handbook.* (Kluwer Academic Pub, 2002).
193. De Santis, M. M. *et al.* Extracellular-Matrix-Reinforced Bioinks for 3D Bioprinting Human Tissue. *Advanced materials (Deerfield Beach, Fla.)* **n/a**, 2005476.
194. Dubbin, K., Tabet, A. & Heilshorn, S. C. Quantitative criteria to benchmark new and existing bio-inks for cell compatibility. *Biofabrication* **9**, 044102, (2017).
195. Kolesky, D. B. *et al.* 3D bioprinting of vascularized, heterogeneous cell-laden tissue constructs. *Adv. Mater.* **26**, 3124-3130, (2014).
196. McAuley, J. R. & Anand, V. K. Clinical significance of compound cilia. *Otolaryngology - Head and Neck Surgery* **118**, 685-687, (1998).
197. Pinto, A. L., Rai, R. K., Hogg, C. & Burgoyne, T. Ciliary Feature Counter: A program for the Quantitative Assessment of Cilia to Diagnose Primary Ciliary Dyskinesia. *Diagnostics (Basel, Switzerland)* **10**, (2020).
198. Burgersdijk, F. J., De Groot, J. C., Graamans, K. & Rademakers, L. H. Testing ciliary activity in patients with chronic and recurrent infections of the upper airways: experiences in 68 cases. *The Laryngoscope* **96**, 1029-1033, (1986).
199. Jiang, D. *et al.* Two succeeding fibroblastic lineages drive dermal development and the transition from regeneration to scarring. *Nat. Cell Bio.* **20**, 422-431, (2018).
200. Turner, N. J. & Badylak, S. F. The Use of Biologic Scaffolds in the Treatment of Chronic Nonhealing Wounds. *Adv. Wound Care* **4**, 490-500, (2015).
201. Wu, J., Ravikumar, P., Nguyen, K. T., Hsia, C. C. W. & Hong, Y. Lung protection by inhalation of exogenous solubilized extracellular matrix. *PLoS One* **12**, e0171165, (2017).
202. Boyden, E. A. A critique of the international nomenclature on bronchopulmonary segments. *Diseases of the chest* **23**, 266-269, (1953).
203. Lin, L., Spoor, M. S., Gerth, A. J., Brody, S. L. & Peng, S. L. Modulation of Th1 Activation and Inflammation by the NF-κB Repressor Foxj1. *Science* **303**, 1017-1020, (2004).
204. Parker, M. W. *et al.* Fibrotic extracellular matrix activates a profibrotic positive feedback loop. *The Journal of clinical investigation* **124**, 1622-1635, (2014).
205. Godin, L. M. *et al.* Decreased Laminin Expression by Human Lung Epithelial Cells and Fibroblasts Cultured in Acellular Lung Scaffolds from Aged Mice. *PloS one* **11**, e0150966, (2016).
206. Gilpin, S. E. *et al.* Fibrillin-2 and Tenascin-C bridge the age gap in lung epithelial regeneration. *Biomaterials* **140**, 212-219, (2017).

207. Medina, R. J. *et al.* Myeloid angiogenic cells act as alternative M2 macrophages and modulate angiogenesis through interleukin-8. *Molecular medicine (Cambridge, Mass.)* **17**, 1045-1055, (2011).
208. Snyder, R. J. *et al.* Macrophages: A review of their role in wound healing and their therapeutic use. *Wound repair and regeneration : official publication of the Wound Healing Society [and] the European Tissue Repair Society* **24**, 613-629, (2016).
209. Ciccone, G. *et al.* What Caging Force Cells Feel in 3D Hydrogels: A Rheological Perspective. *Advanced healthcare materials*, e2000517, (2020).
210. Cuomo, F., Cofelice, M. & Lopez, F. Rheological Characterization of Hydrogels from Alginate-Based Nanodispersion. *Polymers (Basel)* **11**, 259, (2019).
211. Zuidema, J. M., Rivet, C. J., Gilbert, R. J. & Morrison, F. A. A protocol for rheological characterization of hydrogels for tissue engineering strategies. *J. Biomed. Mater. Res. B* **102**, 1063-1073, (2014).
212. Renier, N. *et al.* iDISCO: A Simple, Rapid Method to Immunolabel Large Tissue Samples for Volume Imaging. *Cell* **159**, 896-910, (2014).
213. Paul, H., Reginato, A. J. & Ralph Schumacher, H. Alizarin red s staining as a screening test to detect calcium compounds in synovial fluid. *Arthritis Rheum.* **26**, 191-200, (1983).
214. Titford, M. The long history of hematoxylin. *Biotechnic & histochemistry : official publication of the Biological Stain Commission* **80**, 73-78, (2005).